Molecular Therapy
Review

# Non-invasive Reporter Gene Imaging of Cell Therapies, including T Cells and Stem Cells

Candice Ashmore-Harris,[1,2] Madeleine Iafrate,[1,5] Adeel Saleem,[1,3,4,5] and Gilbert O. Fruhwirth[1]

[1]Imaging Therapy and Cancer Group, Department of Imaging Chemistry and Biology, School of Biomedical Engineering and Imaging Sciences, King's College London, London SE1 7EH, UK; [2]Centre for Stem Cells and Regenerative Medicine, School of Basic and Medical Biosciences, King's College London, London SE1 9RT, UK; [3]Peter Gorer Department of Immunobiology, School of Immunology and Microbial Sciences, King's College London, London SE1 9RT, UK; [4]Department of Haematological Medicine, King's College Hospital, London SE5 9RS, UK

**Cell therapies represent a rapidly emerging class of new therapeutics. They are intended and developed for the treatment of some of the most prevalent human diseases, including cancer, diabetes, and for regenerative medicine. Currently, they are largely developed without precise assessment of their *in vivo* distribution, efficacy, or survival either clinically or preclinically. However, it would be highly beneficial for both preclinical cell therapy development and subsequent clinical use to assess these parameters *in situ* to enable enhancements in efficacy, applicability, and safety. Molecular imaging can be exploited to track cells non-invasively on the whole-body level and can enable monitoring for prolonged periods in a manner compatible with rapidly expanding cell types. In this review, we explain how *in vivo* imaging can aid the development and clinical translation of cell-based therapeutics. We describe the underlying principles governing non-invasive *in vivo* long-term cell tracking in the preclinical and clinical settings, including available imaging technologies, reporter genes, and imaging agents as well as pitfalls related to experimental design. Our emphasis is on adoptively transferred T cell and stem cell therapies.**

Cell-based therapy, or cell therapy, is defined as the administration of live cell products with the intention of providing effector cells to treat disease or support other treatments. Cell therapies use either cells isolated from the patient (autologous) or those from a donor (allogeneic). The type of therapeutic cell used varies widely, with clinical trials currently dominated by hematopoietic cells, mesenchymal signaling cells,[1] and lymphocytes, but also, at a lesser frequency, dendritic cells, hepatocytes, and epithelial cells with various others also under investigation.[2,3] While cell therapy currently attracts much attention across various fields, it is not a new concept. In 1931, the Swiss medic P. Niehans injected fresh calf parathyroid gland cells into a human female whose own parathyroid gland had been accidentally removed during surgery; she recovered from the procedure. He claimed that embryonic animal cells would be able to regenerate human cells and organs. After more experimentation with fetal cells from black mountain sheep that were apparently resistant to cancer and other diseases, he further claimed that his fresh cell approach could help to cure cancer. However, there was a lack of scientific evidence supporting these claims and the American Cancer Society warned against unproven fresh cell therapies.[4] Allogeneic hematopoietic stem cell transplantation (HSCT) was pioneered by E.D. Thomas[5] to treat leukemia patients, and it evolved to become the standard of care for hematological malignancies and congenital or acquired disorders of the hematopoietic system; it is also a therapeutic option in some solid tumors.[6] Oncology is currently the field responsible for more than half of all cell therapy trials,[2] and there have been several product approvals in recent years.[7–10] Unlike other treatments, cell therapies are live cell products and, via genetic engineering, can be enhanced to achieve better efficacy, or be tailored to benefit individual patients. The first clinically approved genetically engineered cell therapies were the chimeric antigen receptor T cell (CAR-T) therapies tisagenlecleucel and axicabtagene ciloleucel, both of which are autologous CD19-targeted CAR-T immunotherapies for the treatment of certain hematological malignancies (B cell lymphomas[11]). Although spectacular treatment successes have been reported for CAR-T, not all patients respond in this way, and some effects are only temporary;[7,9,12] additionally, CAR-T has so far generally been disappointing in solid tumors.

All cell therapies require extensive characterization to demonstrate safety and compatibility. It is noteworthy that their *in vivo* distribution, survival, and efficacy at on-target tissues, but also off-target tissues, are critical parameters. During clinical trials, off-target activities have led to severe adverse events with fatalities and other life-threatening side effects reported.[13,14] Furthermore, most clinical cell therapy trials are still performed without knowledge about the *in vivo* distribution and fate of the administered therapeutic cells, which has resulted in suggestions to implement *in vivo* cell tracking[15–17] and suicide genes[18] into these genetically engineered cell therapies. Genetic engineering to implement additional payloads (e.g., reporter genes for imaging, suicide genes) into immune cell therapies such as CAR-Ts is less of a regulatory concern compared to genetic engineering of stem cell therapies, given that CAR-expression is enabled by genetic engineering and CAR-Ts are widely used in the clinic. In contrast, the clinical use of

https://doi.org/10.1016/j.ymthe.2020.03.016.

[5]These authors contributed equally to this work.

**Correspondence:** Gilbert O. Fruhwirth, Imaging Therapy and Cancer Group, Department of Imaging Chemistry and Biology, School of Biomedical Engineering and Imaging Sciences, King's College London, Lambeth Wing 4th Floor, Westminster Bridge Road, London SE1 7EH, UK.
**E-mail:** gilbert.fruhwirth@kcl.ac.uk

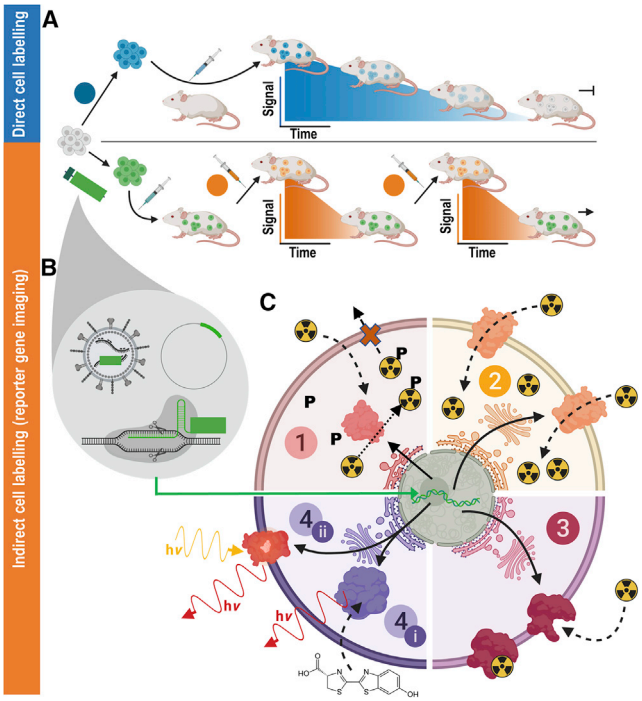


**Figure 1. *In Vivo* Cell Tracking Using Reporter Genes**

(A) (Blue) Direct cell labeling employs *ex vivo*-labeled cells that are administered to animals and can be tracked until cells lose their labels (depicted using blue signal versus time cartoon plots), e.g., through label efflux, via label dilution in fast-growing cells, or radioisotope decay if radiotracers are used. (B) (Orange) Indirect cell labeling requires cells that have been genetically manipulated to express a reporter gene (green). The genetic engineering options frequently employed in reporter gene applications include viruses (e.g., lentiviruses, γ-retroviruses), gene editing, or episomal plasmids (see cartoons within gray drop). The cells are imaged using the features of the reporter gene, which renders the cells traceable *in vivo*. Cells are detected *in vivo* through molecular probe administration (depicted using orange signal versus time cartoon plots); if radiotracers are used, their half-life is short to enable short repeat-imaging intervals and keep administered doses low. Reporter gene imaging does not suffer from label dilution in fast-growing cells and hence permits much longer, theoretically indefinite observation times. (C) Molecular imaging mechanisms of frequently used reporter genes. (1) Enzymes entrapping molecular probes (light red): these reporter enzymes entrap a substrate that is already detectable by imaging. A frequent mechanism for this entrapment relies on phosphorylation of a substrate that has either actively or passively entered the cell, and upon phosphorylation can no longer leave the cell. Examples are nucleoside kinases such as HSV1-*tk*. (2) Transporter proteins (yellow): these reporters are expressed at the plasma membrane of cells, and each expressed reporter can transport several labeling agent molecules into the cell, which constitutes a signal amplification mechanism. The radionuclide transporters NIS and NET belong to this class of reporters. (3) Cell surface molecules (pink): these reporters are expressed at the plasma membrane of cells, and molecular probes bind directly to them; minor levels of signal amplification are theoretically possible if several labels bind directly to each reporter protein, or if several labels could be fused to a reporter binding molecule; however, signal amplification is inferior compared to transporters, and often they are used with a 1:1 stoichiometry. Examples for this reporter class are $tPSMA^{N9Del}$ and SSTR2. (4) Signal generating proteins (purple). (i) Enzyme-based reporters bind to their substrate and catalyze the production of a detectable signal. Examples are luciferases, which convert an externally supplied chemical substrate into detectable light (hν). (ii) Fluorescent proteins contain an intrinsic fluorescence-generating moiety if appropriately excited by light. Fluorophore excitation results in emission of detectable longer wavelength/red-shifted light. For details and literature references to relevant reporter genes, see Tables 1 and 2. The figure was generated using Biorender.com.

genetically modified stem cell therapies is not yet widespread.[19,20] With both types of therapy, there remain several unknowns, including the *in vivo* distribution, persistence, and survival of cells as well as their efficacy at target and non-target sites. Consequently, broader and better investigations into these unknowns during cell therapy development and clinical translation are needed.

## Principles of Non-invasive *In Vivo* Cell Tracking

Depending on the cell therapy being developed, traditional approaches for verifying cell survival *in vivo* relied on methods such as qPCR-based evaluations of cell retention, drug dose escalation, and tumorigenicity tests. The use of molecular imaging permits the acquisition of spatiotemporal whole-body images, meaning that non-invasive *in vivo* tracking of administered therapeutic cells is now possible.[21] Cell tracking enables the quantitative assessment of several crucial aspects for cell therapy development: (1) the whole-body distribution of therapeutic cells over time; (2) whether therapeutic cells migrate beyond the transplant site during treatment, and, if so, the kinetics of this process; (3) whether on-target bystander effects occur; and (4) how long therapeutic cells survive. Notably, cell tracking is based on repeat imaging of the same subjects, and it therefore provides better statistical data through reduced inter-subject variability when compared to conventional approaches that relied on sacrificing animal cohorts at different time points.

### *Signal Formation for* In Vivo *Cell Tracking*

Cell therapies cannot ordinarily be tracked in real time, non-invasively *in vivo* by an imaging technology, without first labeling them. The labeling agent is chosen to match the desired imaging modality (e.g., ultrasound imaging), and it generates a detectable signal in order to provide a noticeable difference between the labeled cells and their surrounding environment. That said, the intrinsic features of some cell types of interest can be exploited to generate trackable signals. For example, when cancer cells express molecules that show low or no expression in other tissues, conventional molecular imaging offers cell-tracking possibilities both preclinically and clinically. As an example, using radiopharmaceutical-based molecular imaging, metastatic cells can be tracked via the sodium iodide symporter (NIS) from the thyroid,[22,23] via the glutamate carboxypeptidase 2 (prostate-specific membrane antigen [PSMA]) from prostate cancer,[24,25] via the carcinoembryonic antigen (CEA) from colorectal cancers,[26] or imaging melanogenic melanomas and their spread.[27]

In most *in vivo* tracking scenarios, cell labels must be introduced to the cells of interest via one of two different methodologies: either direct or indirect cell labeling. Direct cell labeling is performed upon cells *ex vivo*, and the labeled cells are subsequently administered to subjects for cell tracking using the relevant imaging technology (Figure 1A). Uptake of the labeling agent can be achieved by

exploiting normal cellular processes (e.g., through phagocytosis, via internalizing receptors) or assisted (e.g., by transfection agents or coupling of the contrast agent to membrane translocation peptides). A wide variety of ready-to-use contrast agents that are compatible with all relevant imaging technologies are available.[21] Conversely, indirect labeling requires cells to be genetically engineered to ectopically express a reporter gene, rendering them different from the surrounding cells *in vivo* (Figure 1B). The reporter is normally integrated permanently into cells (see Gene Transfer Methods for Reporter Gene Introduction) and it must allow them to be targeted by molecular imaging *in vivo* following administration of a suitable labeling agent. Therefore, the relatively simple process of molecular imaging can be performed repeatedly (whereas the cell labeling only needs to occur once), allowing the genetically modified cells to be tracked longitudinally.

There are three principal strategies that ensure reporter genes afford indirectly labeled cells a detectable signal for *in vivo* imaging. These rely on the reporter gene coding for either an enzyme, cell surface protein, or transport protein (Figure 1C). Where the reporter gene yields expression of a functional enzyme it is catalysis of the administered substrate that renders the cells trackable, e.g., through entrapment of the signal within reporter-expressing cells (e.g., the radiolabeled substrates of herpes simplex virus 1 thymidine kinase [HSV1-*tk*], tyrosinase) or the generation of a signal (e.g., luciferases converting a chemical into detectable light). Cell surface protein-based reporter genes exploit binding of labeling agents for imaging (e.g., receptor binding of a labeled ligand). It is noteworthy that some reporter proteins have enzymatic capacity, but the latter aspect is not utilized for imaging (e.g., PSMA and its variants[28,29] or estrogen receptor[30]). Transporter protein reporters enable a labeled substrate to be transferred into cells to generate a signal. All of these mechanisms can be useful for preclinical cell tracking. However, for clinical cell tracking, the emphasis lies on cell surface proteins, transporters, and enzymes entrapping molecular probes (Figure 1C, parts 1–3), because signal-generating proteins (Figure 1C, part 4) are often either not of human origin (e.g., luciferase) or produce potentially toxic products when expressed outside their endogenous niche (e.g., tyrosinase[31]). A notable exception are certain mammalian nucleoside kinases.[32] Alongside improvements in imaging technologies, corresponding reporter gene-afforded cell labeling agents have been developed and optimized. Reporter genes can either be foreign in relationship to the host organism or represent self; according to these criteria several promising reporter genes are listed in Tables 1 and 2.

### *Gene Transfer Methods for Reporter Gene Introduction*

Traditionally, genetic engineering has been achieved through the use of viral vectors (e.g., γ-retroviruses, lentiviruses), which more or less randomly integrate the transgenes into the genome.[114] This approach is often also classified as "gene therapy" and has been applied for cell therapies in diverse etiologies ranging from cancer immunotherapies to the regulation of immune tolerance in autoimmune diseases.[14] Lentiviruses are capable of efficiently transducing both actively dividing and non-dividing cell types, making them particularly valuable for stable gene transfer to mature somatic cells and lineage-committed, non-proliferating cells (i.e., differentiated from stem cells). In contrast, γ-retroviruses efficiently transduce only actively dividing cells, and they have been commercially approved for use in gene therapy applications for *ex vivo* modification of T cells and hematopoietic stem cells.[115] Random genomic integration is associated with the risk of altering normal gene function at or around the integration site. Moreover, effects on the inserted reporter cannot be ruled out nor can epigenetic silencing. To mitigate this, episomal plasmids have also been used, which can yield stable transgene expression (e.g., when delivered by transfection or electroporation[116,117]). Gene editing, a form of genetic engineering, offers a much more specific way of integrating a desired genetic payload at a distinct location into the genome of target cells.[118,119] Provided that a suitable integration site is selected, this can enable stable reporter gene expression even in instances where there is high proliferation. This is of particular utility in the context of stem cell therapies, where random integration of therapeutic, reporter, and suicide genes would pose risks of both insertional mutagenesis and downstream silencing. In fact, gene editing is already in use clinically for a range of cell therapies due to these inherent advantages.[20]

## Experimental Design Considerations for Indirect Cell Tracking

Planning reporter gene-afforded (indirect) *in vivo* cell-tracking experiments requires careful consideration of diverse parameters such as whether the study is staged in a preclinical or clinical setting, whether immunocompetent or immunocompromised host organisms will be used, the type of imaging technology, desired therapeutic cell detection sensitivity, overall observation period and desired imaging intervals, and labeling agent availability.

### *Cell Detection Sensitivity*

Exquisite detection sensitivity is required for *in vivo* cell tracking. It is dictated by both the choice of reporter gene and its corresponding contrast agent as well as the matched imaging technology.

First, the reporter-signal pair must be detected by a matching imaging technology. Ideally, it should offer molecular sensitivities in, or below, the picomolar concentration range (Figure 2). The most suitable imaging technologies are therefore bioluminescence and radionuclide modalities; only in special cases can other imaging technologies fare as well for *in vivo* cell tracking. For example, tracking of melanin-producing murine melanoma cell spread was achieved in mice at reasonable sensitivity and resolution compared to the study goals by using photoacoustic tomography.[120] Importantly, many disease models require 3D tomographic imaging in rodents or larger mammals, i.e., non-translucent organisms. Consequently, optical imaging technologies are unfavorable due to their inherent limitations relating to light scattering and absorption by tissues. While extremely sensitive, bioluminescence cannot provide accurate and reliable 3D information. Hence, radionuclide imaging modalities are generally preferable for *in vivo* cell tracking from this perspective.

**Table 1. Promising Host-Compatible Reporter Genes and Their Corresponding Imaging Tracers**

| Reporter | | | | Imaging Agent | | |
|---|---|---|---|---|---|---|
| Class | Name | Properties | aa[a] | Modality | Properties | Refs. |
| Transporter | sodium iodide symporter (NIS, SLC5A5) | symports $Na^+$ alongside various anions; endogenous expression in thyroid, stomach, lacrimal, salivary, and lactating mammary glands, small intestine, choroid plexus, and testicles | 618 | PET: $^{124}I^-$, [$^{18}$F]$BF_4^-$, [$^{18}$F]$SO_3F^-$, [$^{18}$F]$PF_6^-$; SPECT: $^{99m}TcO_4^-$, $^{123}I^-$ | tracers do not cross the blood-brain barrier (BBB); several tracers are clinically approved, most require no cyclotron ($^{99m}TcO_4^-$/$^{xy}I^-$) or are made by automated synthesis[33] | 34–36,37,38 |
| | norepinephrine transporter (NET, SLC6A2) | NaCl-dependent monoamine transporter; endogenously expressed in organs with sympathetic innervation (heart, brain) | 617 | PET: [$^{124}$I]MIBG,[b] [$^{11}$C] hydroxyephedrine; SPECT: [$^{123}$I]MIBG[b] | tracers do not cross the BBB | 39 |
| | dopamine transporter (DAT, SLC6A3) | NaCl-dependent | 620 | PET: [$^{11}$C]CFT, [$^{11}$C]PE2I, [$^{18}$F]FP-CIT; SPECT: $^{123}$I-β-CIT,[b] $^{123}$I-FP-CIT,[b] $^{123}$I-ioflupane,[b] $^{99m}$TRODAT | few data in the public domain; tracers cross the BBB. | 40 |
| Enzyme | pyruvate kinase M2 | expression during development, also in cancers | 531 | PET: [$^{18}$F]DASA-23 | background in organs of excretion route; suggested for cell tracking within brain; tracer crosses the BBB | 41 |
| | thymidine kinase (hmtk2/hΔTK2) | human kinase causing cellular tracer trapping | 265 | PET: [$^{124}$I]FIAU,[b] [$^{18}$F] FEAU, [$^{18}$F]FMAU (for hTK2-N93D/L109F) | tracers do not cross the BBB; endogenous signals in gall bladder, intestine, and organs involved in clearance | 42 |
| | deoxycytidine kinase (hdCK) | human kinase causing cellular tracer trapping | 260 | PET: [$^{124}$I]FIAU,[b] [$^{18}$F] FEAU | tracers do not cross the BBB; endogenous signals in gall bladder, intestine, and organs involved in clearance | 32,43 |
| Cell surface receptor | somatostatin receptor type 2 (SSTR2) | G protein-coupled receptor; endogenous expression in brain, adrenal glands, kidneys, spleen, stomach, and many tumors (i.e., SCLC, pituitary, endocrine, pancreatic, paraganglioma, medullary thyroid carcinoma, pheochromocytoma) | 369 | PET: $^{68}$Ga-DOTATOC, $^{68}$Ga-DOTATATE; SPECT: $^{111}$In-DOTA-BASS (best tracers selected here) | tracers may cause cell signaling, change proliferation, and might inhibit/impair cell function; non-metal octreotide radiotracers can cross the BBB; some tracers clinically approved; $^{68}$Ga/$^{111}$In-based tracers are readily accessible | 44–47 |
| | dopamine receptor ($D_2R$) | G protein-coupled receptor; high endogenous expression in pituitary gland and striatum | 443 | PET: [$^{18}$F]FESP, [$^{11}$C] raclopride, [$^{11}$C]*N*-methylspiperone | slow clearance of [$^{18}$F]FESP; tracers cross the BBB | 48–51 |
| | transferrin receptor (TfR) | fast recycling receptor | 760 | MRI: transferrin-conjugated SPIO | transferrin-conjugated SPIO particles are internalized by cells | 52 |

(*Continued on next page*)

**Table 1. *Continued***

| Reporter | | | | Imaging Agent | | |
|---|---|---|---|---|---|---|
| Class | Name | Properties | aa[a] | Modality | Properties | Refs. |
| Cell surface protein | glutamate carboxy-peptidase 2 (PSMA) and variant tPSMA$^{N9Del}$ | tPSMA$^{N9Del}$ has higher plasma membrane concentration; high expression in prostate | 750 | PET: [$^{18}$F]DCFPyL, [$^{18}$F]DCFBC; SPECT: [$^{125}$I]DCFPyL[b]; anti-PSMA antibodies and ligands can be flexibly labeled[a]; e.g., J951-IR800 | background signal in kidneys; tracers do not cross the BBB; ome tracers clinically approved | 28,29 |
| Cell surface-antigen | human carcinoembryonic antigen-based reporters | CEA expressed in pancreatic, gastric, colorectal, and medullary thyroid cancers; reporters are recombinant proteins based on CEA minigene (N-A3) fused to extracellular and transmembrane domains of human FcγRIIb receptor, CD5, or TfR carboxyl-terminal domain | ca. 460 | PET: $^{124}$I-anti-CEA scFv-Fc H310A,[b] [$^{18}$F]FB-T84.66 diabody; SPECT: $^{99m}$Tc-anti-CEA Fab′, $^{111}$In-ZCE-025, $^{111}$In-anti-CEA F023C5i[c] | tracers do not cross the BBB; $^{99m}$Tc-anti-CEA Fab′ is clinically approved | 53,54,55–57 |
| Artificial cell surface molecule | DOTA antibody reporter 1 (DAbR1) | scFv of murine anti-DOTA IgG1 antibody 2D12.5/G54C fused to human IgG4 CH2-CH3 and the transmembrane domain of human CD4 | ca. 470 | PET: $^{86}$Y-AABD | $^{86}$Y-AABD is a DOTA complex that binds irreversibly to a cysteine of 2D12.5/G54C; tracer does not cross the BBB | 58 |
| | estrogen receptor α ligand binding domain (hERL) | no reported physiological function; endogenous estrogen receptor expression limited to uterus, ovaries, and mammary glands | estimate250[d] | PET: [$^{18}$F]FES | tracer is clinically used estrogen receptor imaging agent; imaging agent crosses the BBB | 30 |
| | anti-PEG Fab fragment | recombinant protein with N-terminal hemagglutinin (HA)-tag, anti-PEG Fab, followed by a c-myc epitope and eB7; tags could cause immunogenicity | 812 | PET: $^{124}$I-PEG-SHPP[b,c]; MRI: SPIO-PEG; fluorescence, e.g., NIR797-PEG | iodine tracers bear risk of deiodination; some tracers cross the BBB; PEG is non-toxic and approved by the US Food and Drug Administration (FDA) | 59 |
| Carrier protein | ferritin | human heavy and light chains co-expressed, or murine heavy chain only expressed as reporter | Hu: 183/175 | MRI: iron | iron is not equally distributed across the brain and therefore may cause local susceptibility shifts that are above the MRI detection limit | 60,61 |

Promise was evaluated by the authors based on (1) human reporter origin ensuring no immunogenicity against the therapeutic cells expressing the reporter, and (2) availability of at least one already clinically approved or first-in-man tried labeling agent.

[a]Amino acid chain length as an indication of reporter molecular weight (MW; not accounting for posttranslational modifications); wild-type reporter MWs are indicated.

[b]Radioiodinated tracers can become de-iodinated *in vivo*, resulting in free iodide that is subsequently taken up into NIS-expressing organs.

[c]Any other modality can be used provided a suitable contrast-forming moiety will be attached to PEG and the CEA antibodies, respectively.

[d]Report[30] does not clearly describe reporter construction, leaving precise reporter size only to be estimated; we estimate it based on the estrogen receptor α ligand binding domain, which is approximately 250 aa long (cf. http://pfam.xfam.org/family/PF02159).

**Table 2. Non-mammalian Reporter Genes and Their Corresponding Imaging Tracers**

| Reporter | | | | Imaging Agent | | |
|---|---|---|---|---|---|---|
| Class | Name | Properties | aa[a] | Modality | Properties | Refs. |
| Enzyme | β-galactosidase | glycoside hydrolase enzyme; product of LacZ gene and isolated from *E. coli* | 1,021 | optical CL: near-infrared dioxetane luminophores (emission λ = 690 nm); MRI: EgadMe[b]; PET: 2-(4-[$^{123}$I]iodophenyl)ethyl-1-thio-β-D-galactopyranoside, 3-(2′-[$^{18}$F]fluoroethoxy)-2-nitrophenyl-β-D-galactopyranoside, 3-[$^{11}$C]methoxy-2-nitrophenyl-β-D-galactopyranoside; [$^{18}$F]FPyGal; SPECT: 5-[$^{125}$I]iodoindol-3-yl-β-D-galactopyranoside ([$^{125}$I]IBDG); 4-chloro-3-bromoindole-galactose (X-gal) | cellular toxicity depending on the substrates; lack of sensitivity and high background; rapid renal clearance of [$^{125}$I]IBDG impedes intratumoral availability if systemically administered | 62–68 |
| | *E. coli* dihydrofolate reductase (eDHFR) | catalyzes NADPH-dependent reduction of folate; inhibited by highly specific small molecule trimethoprim | 159 | PET: [$^{11}$C]trimethoprim, [$^{18}$F]trimethoprim (TMP) | rapid renal clearance and hepatobiliary metabolism | 69,70 |
| | HSV1-*tk* and mutants | kinase causing cellular tracer | 376 | PET: [$^{124}$I]FIAU, [$^{18}$F]FEAU, [$^{18}$F]FHBG | tracers do not cross the blood-brain barrier | 71–75 |
| | emerald luciferase (ELuc) and mutants | catalyzes oxygenation of D-luciferin to oxyluciferin; emits strongest luminescence among beetle luciferases; from click beetle (*Pyrearinus termitilluminans*) | 543 | optical BL: D-luciferin/ATP (emission λ = 534–626 nm; dependent on wild-type [WT]/mutant used) | lack of signal in the brain, as the substrate cannot cross the BB barrier; low thermostability and low light intensity | 76–79 |
| | firefly luciferase (fLuc) and mutants | catalyzes the oxygenation of D-luciferin to oxyluciferin; derived from the North American firefly (*Photinus pyralis*) | 550 | optical BL: D-luciferin/ATP (emission λ = 550–615 nm; depending on WT/mutant used) | depending on the type used; high thermolability and exhibits a bathochromic shift at >30°C and pH levels <7.8 | 80,81,82 |
| | *Gaussia* luciferase (GLuc) and mutants | from *Gaussia princeps*; one of the smallest luciferases cloned so far; catalyzes the oxidative decarboxylation of coelenterazine to produce luminescence | 185 | optical BL: coelenterazine (emission λ = 480–513 nm; depending on WT/mutant used) | no clinical use; background auto-luminescence | 83–86 |
| | green click beetle luciferase and mutants | derived from *Pyrophorus plagiophthalamus* | 542 | optical BL: luciferin (emission λ = 543) | no clinical use | 87 |
| | NanoLuc | derived from *Oplophorus gracilorostris* (deep sea shrimp) | 171 | optical BL: imidazopyrazinone substrate (furimazine) (emission λ = 456 nm) | signal is heavily attenuated in tissues | 88–91 |
| | *Renilla* luciferase (RLuc) and mutants | derived from *Renilla reniformis* (sea pansy) | 311 | optical BL: coelenterazine (emission λ = 475–535 nm; depending on the variant) | WT RLuc suffers from low stability in serum and thermolability at >30°C | 81,92,93 |
| Transporter | MS-1 *magA* | putative ion transport protein from magnetotatic bacteria (*Magnetospirillum* sp. strain AMB-1) | 434 | MRI: endogenous or exogenous Fe | delay of change in signal, which is dependent on Fe availability | 94–96 |
| | sodium-taurocholate cotransporting polypeptide (NTCP) | | 349 | MRI: indocyanine green (ICG) | | 97 |

(*Continued on next page*)

**Table 2. *Continued***

| Reporter | | | | Imaging Agent | | |
|---|---|---|---|---|---|---|
| Class | Name | Properties | aa[a] | Modality | Properties | Refs. |
| Artificial protein | lysine-rich protein | frequency-selective contrast, based on transfer of radiofrequency labeling from the reporter's amide protons to water protons | 200 | MRI: chemical exchange saturation transfer (CEST) MRI | | 98,99 |
| Fluorescent proteins | mNeptune | fluorescent protein chromophore; derived from *Entacmaea quadricolor* | 244 | optical FL: (emission λ = 650 nm) | no clinical use | 100 |
| | mPlum | fluorescent protein chromophore; derived from DsRed of *Discosoma* (sea anemone) | 226 | optical FL: (emission λ = 649 nm) | no clinical use; low acid sensitivity | 101 |
| | mTagRFP | fluorescent protein chromophore; derived from *Entacmaea quadricolor* | 238 | optical FL: emission λ = 584 nm | no clinical use | 102 |
| | E2-Crimson | derived from DsRed-Express2 | 225 | optical FL: emission λ = 543 nm | no clinical use | 103,104 |
| NIR fluorescent protein | iFP1.4 | requires exogenously added biliverdin as a co-factor; derived from *Deinococcus radiodurans* | 328 | optical FL: emission λ = 708 nm | no clinical use | 105,106 |
| | iRFP 670 | endogenous biliverdin sufficient as a co-factor; derived from *Rhodopseudomonas palustris* (CGA009) | 312 | optical FL: emission λ = 670 nm | no clinical use | 105,107,108 |
| | iRFP 713 | endogenous biliverdin sufficient as a co-factor; derived from *Rhodopseudomonas palustris* | 317 | optical FL: emission λ = 713 nm | no clinical use | 105,107–109 |
| | iRFP 720 | endogenous biliverdin sufficient as a co-factor; derived from *Rhodopseudomonas palustris* | 317 | optical FL: emission λ = 720 nm | no clinical use | 110,111 |
| Gas-filled protein complex | gas vesicle structural protein A/gas vesicle protein C | gas vesicles generate contrast; gas vesicles occupy more than 10% of the volume of transduced cells | GvpA: 71 | ultrasound: 2.7–4.7 MPa insonation | | 112,113 |
| | | GvpA; derived from *Dolichospermum lemmermannii*; GvpC; derived from *Dolichospermum flosaquae* | GvpC: 193 | | | |
| | mammalian acoustic reporter gene (mARG) | gas vesicles generate contrast | 2,500 | ultrasound: 3.2 MPa insonation | | 112 |

CL, chemiluminescence; BL, bioluminescence; FL, fluorescence imaging.
[a]Amino acid chain length as an indication of reporter molecular weight (MW; not accounting for posttranslational modifications); wild-type reporter MWs are indicated.
[b]EgadMe: 1-(2-(β-galactopyranosyloxy)propyl)-4,7,10-tris(carboxymethyl)-1,4,7,10-tetraazacyclododecane)gadolinium(III).

Second, cell detection sensitivity depends on reporter expression levels and the molecular imaging mechanism underlying its targeting by the imaging agent (Figure 1C). Transporters (e.g., NIS or norepinephrine transporter [NET]) provide signal amplification, as each reporter protein can transport several radiotracer molecules into the cell. Taking NIS as an example, its endogenous expression is highest in thyroid cells, whereas ectopic expression as a transgenic reporter protein in non-thyroidal cells occurs within a mechanistically distinct environment. In these circumstances, iodide radiotracers are not metabolized into thyroid hormones,[22] and consequently radioiodide is subject to different cell residence times and efflux kinetics. NIS is also promiscuous in anion selection for uptake, which has enabled

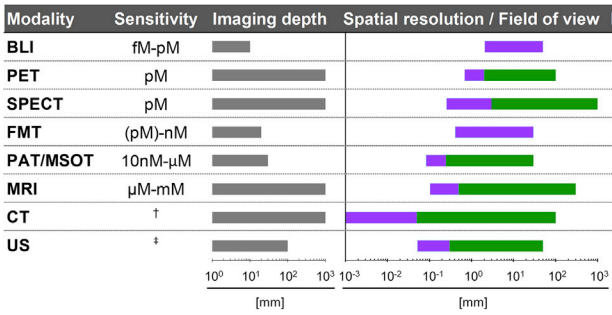


**Figure 2. Properties of Various Whole-Body Imaging Modalities**

Imaging modalities are ordered according to their molecular detection sensitivities with achievable imaging depth shown in gray alongside. Achievable spatial resolution (left end) and fields of view (right end) are shown in cyan/green. Where bars are green, they overlay purple bars and indicate the same parameters but achievable with instruments available for clinical imaging. Instrument cost estimations are classified as follows: $, <$130,000; $$, $130,000–$300,000; $$$, >$300,000. †Contrast agents sometimes used to obtain different anatomical/functional information. ‡Sensitivity is highly dependent on contrast-forming features/contrast agent. A new mammalian reporter gene for US imaging was recently reported to detect a minimum of 135 gas vesicles per voxel with dimensions of 100 μm.[112] &Dual-isotope PET is feasible but not routinely in use; it requires two tracers, one with a positron emitter (e.g., $^{18}$F, $^{89}$Zr) and the other with a positron-gamma emitter (e.g., $^{124}$I, $^{76}$Br, $^{86}$Y), and is based on recent reconstruction algorithms to differentiate the two isotopes based on the prompt-gamma emission.[121–123] %Multichannel MRI imaging has been shown to be feasible[124] but is not routinely available. #Generated by positron annihilation (511 keV). BLI, bioluminescence imaging; PET, positron emission tomography; SPECT, single-photon emission computed tomography; FMT, fluorescence molecular tomography; PAT/MSOT, photoacoustic tomography/multispectral optoacoustic tomography; MRI, magnetic resonance imaging; NIR, near-infrared; VIS, visible; HF, high-frequency; CT, computed tomography.

the development of iodine-free single-photon emission computed tomography (SPECT) and positron emission tomography (PET) tracers, such as $^{99m}TcO_4^-$ (SPECT), $[^{18}F]BF_4^-$, $[^{18}F]SO_3^-$, or $[^{18}F]PF_6^-$ (PET) having recently been reported as alternatives with proof of principle shown in animal models.[34–36,125] These benefit from better decay properties and avoid the drawbacks of undergoing cellular entrapment and metabolization in the thyroid, relative to earlier radioiodide tracers. Reporters that enzymatically entrap radiotracers that are taken up into cells by different mechanisms also offer high cell detection sensitivities due to molecular probe accumulation. Examples include the cytosolic thymidine and cytidine kinases (Tables 1 and 2), which irreversibly phosphorylate the radiotracers when inside (mammalian) cells, thus preventing the radiotracers from being transported back out of the cells. A potential drawback is that these kinases could potentially shift the relevant biochemical equilibria in cells, as they also accept the natural substrates, which could alter cell metabolism; however, systematic studies investigating this aspect are currently not available. Non-enzymatic cell surface molecules such as receptors tend to be less sensitively detected, because they form one-to-one complexes when bound to their molecular probes. Moreover, they can get internalized upon ligand binding, which then impacts detection sensitivity through reduction of their steady-state concentration on the plasma membrane (e.g., human somatostatin receptor 2 [SSTR2][4]). Importantly, the molecular imaging mechanisms should not be regarded in isolation, and other aspects, for example endogenous reporter expression or corresponding probe excretion properties, are additional crucial aspects to achieve good target-to-background ratios (see examples in Cell Tracking in T Cell Therapy Development).

The detection sensitivities of NIS-expressing extra-thyroidal cells have been reported preclinically to be as good as hundreds/thousands for cancer cells expressing NIS *in vitro*,[126,127] and CAR-Ts expressing PSMA *in vitro* and *in vivo*,[29] or tens of thousands for effector T cells using various different reporter genes *in vivo*.[128] Notably, the human NET was found to most sensitively detect reporter-expressing T cells in a direct reporter comparison study between various nucleoside kinases and the transporters NIS and NET;[128] however, the endogenous NET expression and background signals generally obtained by NET imaging are not favorable for T cell tracking (Table 1). As reporter expression levels are cell type-dependent, it is advisable to determine their sensitivities on existing instrumentation.

### *Resolution*

Currently, the imaging methodologies providing best sensitivities are not at the forefront in terms of resolution, providing only millimeter resolution. An exception is fixed-collimator SPECT instrumentation, which has been reported to offer preclinical resolutions of 0.25 mm,[129] albeit at rather long image acquisition times. In contrast, exquisite resolution is offered by computed tomography (CT) and magnetic resonance imaging (MRI), but neither is suitable for generating sufficient contrast in reporter gene-afforded cell tracking at present. The strengths of both have been exploited through combination imaging approaches with highly sensitive radionuclide and bioluminescence technologies, a concept termed multi-modal imaging.[130,131] In multi-modal imaging, the higher resolution anatomical images complement the high-sensitivity images, and the resultant combined images thus enable detected signals to be more readily attributed to their anatomical context when reconstructed. For *in vivo* cell tracking, multi-modal imaging is now the norm with SPECT/CT, PET/CT, PET/MRI, and bioluminescence/CT routinely used preclinically, and both PET/CT and PET/MRI are advantageous in the clinical setting.

### *Observation Time and Interval*

Reporter gene-afforded cell tracking is superior to direct cell-labeling methods in terms of observation time, as it does not suffer from label dilution effects or depend on long-term contrast agent presence (and thus is not affected by contrast agent efflux) (Figures 1A and 1B). This renders reporter gene methods particularly suitable for tracking cells longitudinally, and for tracking rapidly dividing cells (e.g., expanding T lymphocyte-derived therapies, teratomas), as the reporter gene is

inherited by progeny cells, giving rise to theoretically indefinite observation times. In practice, observation times are limited by cell survival and the limit of detection (as traceable cells could become so widely distributed at low concentrations that they fall below the limit of detection).

The principle of reporter gene imaging rests on the attribution of imaging signals to the cells expressing the reporter protein (Figures 1B and 1C). The labeling agent used for this application depends on the chosen imaging modality. Focusing on nuclear imaging techniques that provide high sensitivity and are prime for translation to clinical use (as explained in Resolution), the radiotracer must emit photons at a rate that allows detection by SPECT or PET. The rate at which nuclear material emits photons, or decays, defines its half-life; generally, the physical half-life ($\tau$) of the radionuclide chosen should match the half-life of the biological process that will be imaged (for example, the time taken for a radiotracer to penetrate tissues and accumulate in cells). For theoretically indefinite cell tracking, one would need to use a radiotracer with a theoretically indefinite half-life—this is clearly impractical for imaging and for the patient! However, with reporter gene technology, it is now possible to achieve this goal by repeated administration of short-lived (i.e., minutes/hours) radioisotopes, such as $^{18}$F ($\tau$ = 1.8 h). The choice of radionuclide is of paramount importance. It is important to choose a reporter gene-signal pair offering optimal repeat imaging intervals (Table 1). For example, there are various radiotracers available for thymidine kinase reporters, including [$^{18}$F]FEAU (2′-deoxy-2′-[$^{18}$F]fluoro-5-ethyl-1-β-D-arabinofuranosyluracil) [$^{123}$I]FIAU (2′-fluoro-2′-deoxy-5′-[$^{123}$I]iodo-1β-D-arabinofuranosyluracil), or [$^{124}$I]FIAU. They have distinct radioisotopes incorporated with differing half-lives, i.e., $^{18}$F ($\tau$ = 1.8 h), $^{123}I^-$ ($\tau$ = 13.2 h), or $^{124}I^-$ ($\tau$ = 4.2 days). With current instrumentation, between four and five half-lives are required for radiotracers to sufficiently decay to undetectable levels for a low enough background signal to permit subsequent imaging sessions (~6% radiotracer left assuming the worst-case scenario of no excretion).[127] Alternatively, radiotracers with very short half-lives are not advantageous, as they could lead to sub-optimal reporter detection (if the radiotracer has a relatively longer circulation time) or make experiments logistically challenging, requiring multiple radiotracer productions on the same day. Therefore, radiotracers with half-lives in the low hour range, for example $^{18}$F or $^{99m}$Tc, appear to be a good compromise for experimental designs requiring imaging intervals of approximately days. While repeat imaging adds experimental complexity when using radionuclide techniques, as the tracer must be prepared for each imaging session (Figure 1B), the short-lived radiotracers offer the additional advantage that cells receive significantly lower doses of radiation compared to using direct cell labeling methods during the same tracking period.

### Cell Viability and Its Impact on Detected Cell-Tracking Signals

Indirect cell tracking using reporter genes is fundamentally linked to cell viability, as only viable cells translate the reporter protein, a process that requires cellular energy. The differing molecular imaging mechanisms (Figure 1C) of different reporter proteins also impact how rapidly changes in cell viability can be detected. First, every reporter protein is subject to production and degradation within the respective cellular environment. These processes are naturally unique to each reporter, and it should be noted that cell biological turnover parameters are poorly understood for most reporters employed for *in vivo* cell tracking. The exceptions are fluorescent proteins, which due to their extensive use in cell biology, have been thoroughly investigated in this respect.[132] There are even fluorescent protein variants reported that change their fluorescence spectrum as a function of the time passed since production, so-called fluorescent timers.[133,134] Other groups have manipulated the turnover kinetics of fluorescent proteins through genetic modification or linked it to distinct cellular events. An example of the latter is the fusion of an oxygen-dependent degradation domain (ODD) to a fluorescent protein; this resulted in rapid fluorescent protein turnover under normoxia but stabilization of the reporter when cells underwent hypoxia.[135] This approach building on the ODD from the hypoxia-inducible factor 1$\alpha$ is generally suitable for cytosolic proteins, and its applicability was earlier demonstrated for a luciferase reporter.[136] However, a caveat of using fluorescent and bioluminescent reporters in hypoxic conditions is that their signal generation is reliant on the presence of oxygen, especially luciferase,[137] and this impacts the quantification of hypoxia, likely underestimating true signals. Interestingly, this was also found to be true for thymidine kinases but not for the β-galactosidase reporter,[137] albeit the latter plays no role for *in vivo* cell tracking. This means that reporter function can depend on the environment in the cell, and potentially can also be exploited to report on distinct cellular conditions.

When interrogating cell viability, it is also worth noting that receptor/membrane-protein-based reporters only require binding of the signal/label. This may lead to the detection of fragmented reporter protein, cell debris, or dying yet still traceable cells, at least until clearance of debris by the organism. Transporter reporter genes overcome this issue, because they require a cellular gradient spanning the plasma membrane of an intact cell. For example, NIS requires an intact $Na^+$ gradient for uptake of radiolabeled anions, which is upheld by cellular $Na^+/K^+$ ATPase,[138] an enzyme requiring ATP for function. Once the $Na^+$ gradient cannot be upheld, e.g., through loss of cellular energy or perforation of cell membranes, NIS-mediated transport is compromised and radiotracer signals for imaging are no longer accumulated in cells. In studies tracking cancer cells, this phenomenon was observed by authors reporting images with tumor cores free of NIS signals, demonstrating that dead and dying cancer cells in the necrotic tumor core were not detected, in line with mechanistic expectations.[126,139,33] This means that transporters report cell viability in a more direct manner, being sensitive to cellular energy depletion and death faster than reporters relying solely on protein presence.

### Host-Compatible Reporters versus Foreign Reporters

The host immune status is a major design parameter for all reporter gene imaging applications, as it is fundamentally intertwined with reporter gene selection and the achievable contrast throughout the

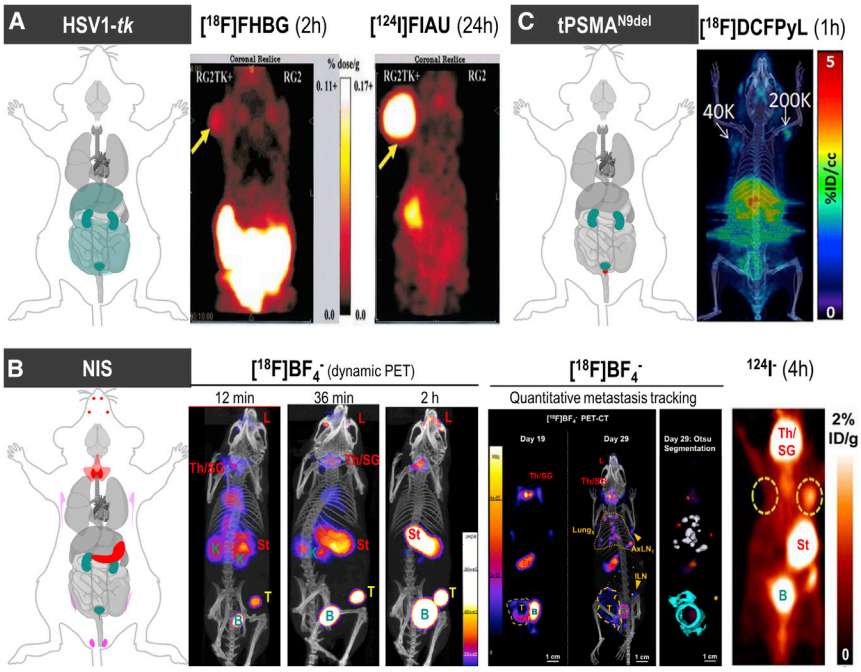


**Figure 3. Background Considerations for Foreign and Host Radionuclide Reporters**

(A) HSV1-*tk* as an example of a foreign reporter is not expressed endogenously in healthy mammals. However, this does not mean that the radiotracer to detect HSV1-*tk*-expressing cells is excluded from background uptake in other mammalian cells/organs or from generating signals during excretion (dark cyan in cartoon). Moreover, it is fundamental for radionuclide imaging that a contrast between background signal and signal arising from reporter-expressing cells (by one of the molecular imaging mechanisms [Figure 1C]) is generated through tissue clearance of radiotracer molecules. Radiotracers can thus affect background differently across different organs as shown here for two different PET radiotracers for HSV1-*tk*. Images are reproduced from a study comparing HSV1-*tk* radiotracer performance,[143] with yellow arrows pointing toward the regions of interest in this study (tumors). Here, the other anatomical sites showing signals are of note (hepatobiliary and renal excretion for [$^{18}$F]FHBG and uptake into the stomach for [$^{124}$I]FIAU). (B) NIS is an example of a host reporter and consequently is expressed endogenously in some organs; NIS is highly expressed in the thyroid and stomach (red), precluding cell tracking from these organs, and at low levels in testes (♂, pink), mammary (♀, pink), and salivary and lacrimal glands (light red). Images shown are from three different studies using varying PET radiotracers for NIS. (B) Left: image demonstrates how [$^{18}$F]$BF_4^-$ *in vivo* distribution changes over time (female mouse with mammary tumor indicated by a yellow "T"; for details, Diocou et al.[127]). (B) Middle: images shown demonstrate metastasis tracking over time and exquisite resolution and sensitivity of NIS-PET imaging for metastasis tracking. They also demonstrate the necrotic tumor core, which is not imaged by NIS due to its favorable dependence on cellular energy for function, thereby reflecting cell viability. An example of Otsu image segmentation is shown to the right, which is the basis for quantitation (for details, see Volpe et al.[33]). Further annotations are endogenous signals from thyroid and salivary glands (Th/SG), stomach (St), and lacrimal glands (L). (B) Right: this image is reproduced from a study elucidating the detection sensitivity of reporter-expressing engineered primary T cells[128] with annotations the same as in the middle images. In both cases radiotracer excretion also leads to signals, in the case of these NIS tracers only from the renal excretion system (K, kidneys, B, bladder). (C) CAR-Ts were engineered to express the tPSMA$^{N9del}$ reporter and administered to NSG mice at the indicated numbers (in 50 μL of 50% Matrigel; white arrows). Imaging with the radiotracer [$^{18}$F]DCFPyL resulted in CAR-T detection. Notably, images are not free of background despite PSMA endogenous expression limited to the prostate (red area in cartoon). This is because radiotracer clearance was incomplete at the point of imaging. To improve the display contrast of the *in vivo* images, the authors masked relatively high renal radiotracer uptake using a thresholding method. For experimental details, see Minn et al.[29] [All data images in this figure are reproduced with minor modifications from the publications mentioned in the legend, with permission from corresponding publishers.]

body. For optimal contrast, a foreign reporter that is expressed nowhere in the host organism would be favorable, as there would be zero background reporter gene expression and therefore no background signal (colloquially referred to as "noise"). Such foreign reporters are, for instance, fluorescent proteins, luciferases[80] or the PET reporter HSV1-*tk*.[140–142] However, the *in vivo* distribution of the labeling agent can cause a level of noise. While this can be avoided with enzyme-activated signals such as those emanating from the luciferase/luciferin reporter/label pair, the situation is different when using radiolabeled agents, since radioactive decay is a physical property that cannot be modulated, activated, or terminated. Consequently, signals detected as a result of radioactive decay must only be interpreted once the radiolabel has had the proper time to circulate, becomes distributed according to its molecular specificity, and is eliminated from other tissues (Figure 3). In practice, this means that even foreign radionuclide imaging reporters are not totally free of background signals; however, unlike bioluminescence, they enable quantitative 3D imaging (Figure 2). Foreign reporter genes have been shown to function in numerous preclinical cell-tracking studies, performed most frequently in heavily immunocompromised animal models.

Where the host organism is immunocompetent or only partly immunocompromised, immunogenicity of the reporter becomes a major experimental design determinant. Any foreign protein, and consequently any cells presenting it (e.g., via major histocompatibility complex [MHC] class I or II), can elicit an immune response (Figure 4). Ultimately, the expression of a foreign reporter molecule can cause the destruction of the administered therapeutic cells by the immune system (Figure 4). Consequently, host-compatible reporters have received considerable attention. These are reporter genes that are from the same species as the host but are endogenously expressed in only a very limited number of host tissues, and ideally at low levels to ensure favorable contrast in adjacent organs (Figure 3). Obviously, the selected host-compatible reporter should not be expressed in organs of interest for the intended cell-tracking study, as this would detrimentally impact the detectability of traceable cells.

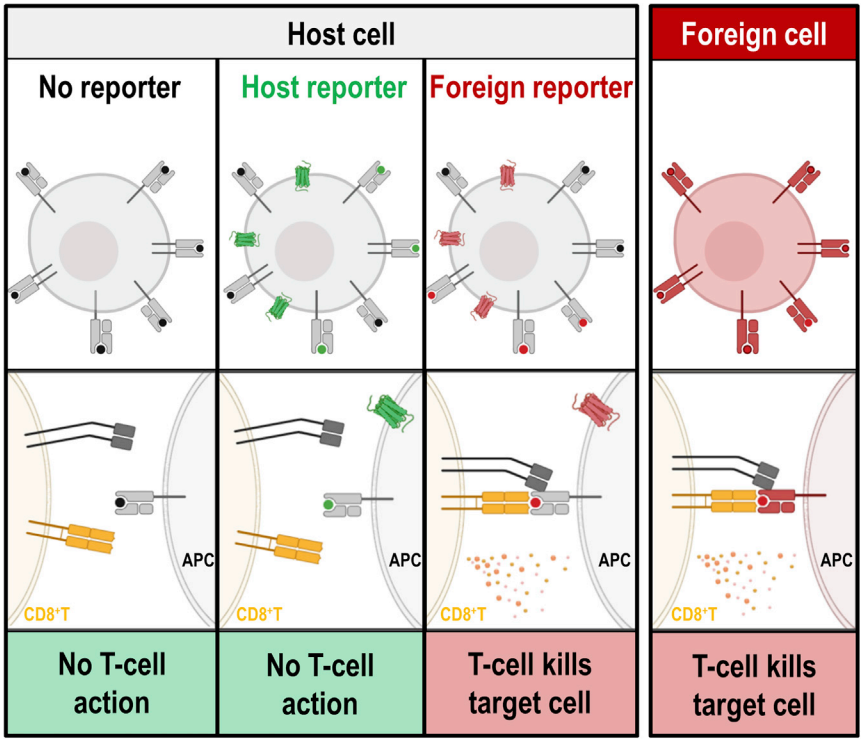


**Figure 4. Recognition of Reporter Antigens by the Immune System**

The intact mammalian immune system operates several mechanisms to recognize cells expressing non-self (i.e., non-host) proteins. As one simplified example, we show here the recognition of antigen-presenting MHC class I molecules on antigen-presenting cells (APCs) by cytotoxic T cells ($CD8^+$Ts). Host cells (far left column, black dots representing presented host antigens) are not recognized by $CD8^+$Ts, as they are pre-coded to not target self. In contrast, non-self MHC class I molecules on foreign cells (far right column) are recognized by $CD8^+$Ts, resulting in destruction of the foreign cells. If host cells express host reporters (center left column, green), corresponding host antigens (green dots) can be presented on MHC class I molecules, and as they are representing self $CD8^+$Ts take no action when they encounter these cells. If foreign reporters are expressed (center right column), self MHC class I molecules present non-self/foreign antigens (red dots), resulting in $CD8^+$T action and killing of the corresponding host cell due to the presence of the foreign reporter. The figure was generated using Biorender.com.

### Cell Tracking in T Cell Therapy Development

Alongside the emergence of anti-cancer immunotherapies, including adoptively transferred T cell immunotherapies, it became necessary to develop methods to image T cells *in vivo*. T cell-specific properties were exploited for this, including cell surface molecules unique to T cells (markers) or specific to particular T cell subsets. Detection of T cells has focused on antibodies or antibody fragments directed against these markers and conjugated to suitable labeling agents (predominantly radioisotopes for high-sensitivity imaging). Examples include: targeting the T cell receptor (TCR[144,145]), the T cell surface glycoprotein cluster of differentiation 3 (CD3[146]), the helper T cell marker CD4, as well as the cytotoxic T cell marker CD8.[147–149] A general limitation to this approach is that the obtained imaging signals cannot be used to back-calculate T cell numbers because the precise expression levels of T cell surface marker molecules are unknown at the point of imaging. As for adoptively transferred T cell immunotherapies, an additional limitation of imaging T cells with molecular probes is the lack of discrimination between the therapeutic cells and host T cells. While the cited examples probe T cell presence, the same limitations exist for methods probing T cell activation.

To overcome this, the adoptively transferred cells were labeled to distinguish them from the resident ones, using both direct and indirect cell labeling approaches, where the general considerations for reporter gene imaging apply. Moreover, T cells are relatively sensitive to radiation-induced damage compared to other cell types (cf. animal irradiation is a routine method to ablate cells of the immune system), hence reporter gene methods that expose labeled cells to lower radiation doses for long-term tracking are even more favorable. Various reporter genes have been used for tracking adoptively transferred T cells. Early studies employed HSV1-*tk* as a reporter gene and demonstrated excellent contrast due to its foreign nature and good sensitivity across the range of its corresponding PET radiotracers (Table 2; Figure 5A). To assess T cell activation, an inducible reporter exploiting the nuclear factor of activated T cells (NFAT; a transcription factor) binding sites for regulation of reporter expression was described.[150] Inducible reporter genes are becoming an important element in the quest to drive reporter gene imaging beyond conventional cell tracking and toward reporting therapeutic activity. To appropriately quantify signal changes, it is best to normalize to an intrinsic constitutive signal, or beacon, which is provided by a second reporter. This concept has been demonstrated repeatedly *in vitro* across various research fields by co-expression using different reporters, for example in oncology and immunology.[87,151–153] Recently, a transgenic mouse has been reported that utilizes two foreign reporters: one luciferase that serves as an NFAT-driven T cell activation marker, and another spectrally different luciferase that operates as a beacon for normalization of T cell signals.[153] HSV1-*tk* has also been chosen for the first proof-of-principle study of reporter gene imaging in humans. This was performed in heavily pre-treated interleukin-13 receptor α2-positive recurrent glioblastoma patients whose prognosis was generally poor;[154] they received $CD8^+$ cytotoxic T lymphocytes (CTLs) engineered to express both the interleukin-13 zetakine chimeric antigen receptor and the reporter.[155] While the CTL tracking was found to be successful, the cohort size was too small to link CTL trafficking and viability to clinical outcome. The above studies were performed in

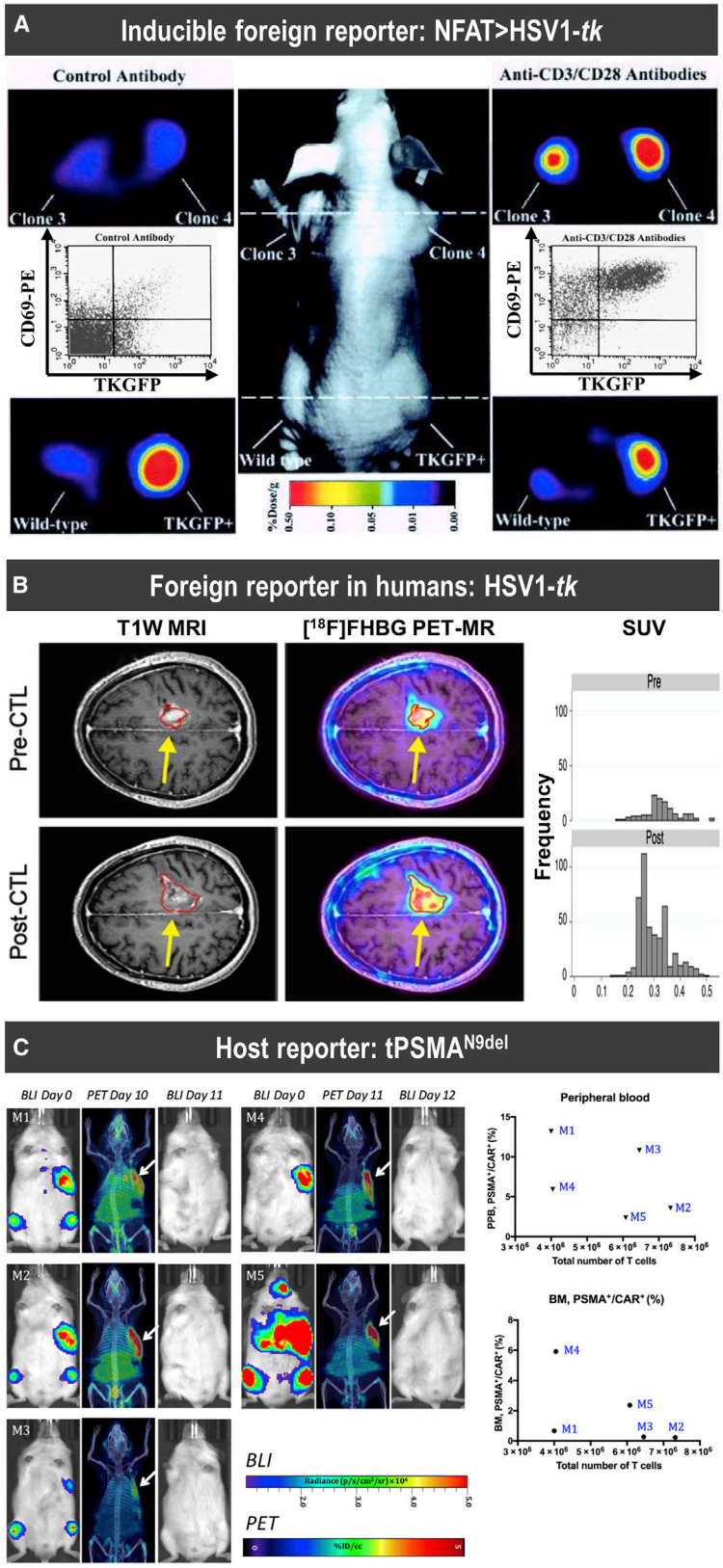


**Figure 5. Examples of Foreign and Host Reporters for T Cell Tracking**

(A) Proof-of-principle study demonstrating non-invasive imaging of T cell activation by NFAT-driven expression of the reporters HSV1-*tk* and GFP (TKGFP) with [$^{124}$I]FIAU as a PET radiotracer for HSV1-*tk*. Photographic image of a typical mouse bearing different subcutaneous infiltrates (middle panel); transaxial PET images of TKGFP expression in a mouse treated with control antibody (left panels) and T cell-activating anti-CD3/CD28 antibodies (right panels) were obtained at the levels indicated by the dashed lines of the middle panel. Samples are the Jurkat/dcmNFATtgn clones 3 and 4 (two similar clones), wild-type Jurkat infiltrates (no reporter control), and Jurkat/TKGFP (constitutive reporter expression as positive control). Gray inset plots show fluorescence-activated cell sorting (FACS) profiles for reporter expression (TKGFP) versus a T cell activation marker (CD69) from a tissue sample obtained from the same Jurkat/dcmNFATtgn clone 4 infiltrate that was imaged with PET above. (B) [$^{18}$F]FHBG PET was performed in a 60-year-old male with multifocal left hemispheric glioma, who received cytotoxic T lymphocytes into the medial left frontal lobe tumor (yellow arrows). Tumor size was monitored by T1-weighted contrast-enhanced MRI (left panels). [$^{18}$F]FHBG PET to detect HSV1-*tk* was recorded and images were fused with MR images (right panels), and 3D volumes of interest were drawn using a 50% [$^{18}$F]FHBG maximum standardized uptake value (SUVmax) threshold, outlined in red. Top row: Images and voxel-wise analysis of [$^{18}$F]FHBG total radioactivity prior to CTL infusion and (bottom row) 1 week after CTL infusion.[155] (C) Longitudinal imaging CAR-T tracking study demonstrating that the number of CD19-tPSMA$^{N9del}$ CAR-T cells in the peripheral blood and the bone marrow does not correlate with the total number of the CD19-tPSMA$^{N9del}$ CAR-Ts localized to the tumors. Left: PET/CT and BLI images of five different mice. Days are marked from the day of CAR-T infusion. Mice were imaged on a SuperArgus small-animal PET/CT 1 h after administration of 14.8 MBq of [$^{18}$F]DCFPyL. Images alternate between fLuc-tagged bioluminescence (BLI, radiance) for visualization of tumor cells and PET/CT for CAR-Ts, with each mouse undergoing both imaging studies. Arrows designate accumulation of CAR-Ts. To improve the display contrast of the *in vivo* images, the relatively high renal radiotracer uptake was masked using a thresholding method. Images are scaled to the same maximum value within each modality. Right: Quantified numbers of the CD19-tPSMA$^{N9del}$ CAR-Ts in the region of interest drawn to cover the entire tumor area were plotted with the percentage number of PSMA$^+$/CAR$^+$ cell populations in the peripheral blood (PPB) and the bone marrow (BM). Each data point (M) represents each mouse. For details, see Minn et al.[29] [Figure modified from publications cited above with permissions obtained.]

immunocompromised animal hosts and heavily pre-treated late-stage cancer patients, respectively, and therefore the documented immunogenicity of HSV1-*tk*[156] has not been a major concern. However, for the development and potential future *in vivo* monitoring of T cell therapies, host-compatible reporters are necessary.

Various host reporters (Figure 4, center left) have been developed, utilizing clinically approved imaging agents that were already available (Table 1). Human SSTR2 has shown some potential for cell tracking based on the existence of clinically approved PET tracers (e.g., [$^{68}$Ga]Ga-DOTATATE, i.e., (1,4,7,10-tetraazacyclododecane-1,4,7,10-tetraacetic acid) [DOTA]-Tyr$^3$-octreotate [antagonist], or [$^{68}$Ga]Ga-DOTATOC, i.e., DOTA-Tyr$^3$-octreotide [agonist]), and it has been used preclinically for CAR-T tracking.[157,158] However, a significant pitfall of using SSTR2 as a reporter is that it is endogenously expressed in various tissues, including the kidneys and gastrointestinal tract,[159] and, importantly, on a variety of immune cell types (T cells, B cells, and macrophages[160]), which negatively affects imaging specificity in immunocompetent models, and likely humans. Furthermore, it was found that the agonist impaired immune function in humans.[161] During imaging, radiotracer concentrations are generally very low, but it cannot be ruled out without further study that somatostatin analogs and its imaging agent derivatives do not impair some immune functions. Another important caveat of the SSTR2 reporter is that it internalizes upon ligand binding,[162,163] thus potentially negatively impacting detection sensitivity (cf. Cell Detection Sensitivity ). Mammalian NIS has been used in a variety of cell-tracking applications in animal models spanning a wide range of different cell types.[126,164–172] This is a testament to both its excellent contrast in many applications, as NIS is only endogenously expressed in the thyroid and a few extra-thyroidal tissues (salivary glands, mammary glands, stomach and small intestine, testes[22]), and its small anionic radiotracers being readily available for both PET and SPECT imaging (Table 1). Notably, if NIS is used together with non-iodine radiotracers such as [$^{18}$F]$BF_4^-$, the signal-to-background ratio is favorable compared to iodide tracers.[127] Recently, NIS has also been exploited in preclinical models for CAR-T therapy tracking, focused on trafficking to prostate cancer and breast cancer models.[173,174] PSMA has also been developed as a reporter gene,[28] mainly due to its extremely limited endogenous expression and the fact that several clinically approved radiotracers for imaging are available, which were originally intended for molecular imaging of PSMA-expressing prostate cancers and their metastases.[175] Interaction of PSMA with its ligand can also result in its internalization,[175,176] which is sensitive to certain amino acid modifications at the N terminus of PSMA.[177] For its use as a reporter gene, a PSMA variant was designed to prevent its internalization and increase its surface expression while also lacking the putative intracellular signaling motifs. This engineered tPSMA$^{N9Del}$ variant has been used to track CAR-Ts in an acute lymphoblastic leukemia model by PET using an $^{18}$F-radiolabelled version of its high-affinity ligand DCFPyL.[29] Interestingly, the authors reported that CAR-T signals obtained from tumors did not correlate with easily accessible peripheral CAR-T blood counts or CAR-T presence in the bone marrow, demonstrating the importance of spatiotemporal cell therapy imaging for accurate monitoring of CAR-T trafficking (Figure 5C).

Another route to reporters with low immunogenicity and good contrast features is to generate artificial proteins consisting of host proteins or their domains. To achieve targeting of these chimeras, incorporation of antibody fragments as extracellular domains that can be targeted with corresponding labeling agents have been reported. For example, murine and human monovalent anti-polyethylene glycol (PEG) fragments without Fc portions have been developed as reporter genes with corresponding labeling agents based on PEG conjugated to a range of diverse labeling agents ($^{124}$I for PET, superparamagnetic iron oxide nanoparticles for MRI, and a near-infrared fluorophore for optical imaging).[59] These approaches were benchmarked for imaging specificity relative to HSV1-*tk*, and similar results were seen. However, they have yet to be tested in T cells. In a similar approach, a single-chain variable fragment (scFv) of the murine anti-lanthanide-DOTA immunoglobulin G (IgG)1 antibody 2D12.5/G54C[178,179] was fused with a human IgG4-CH2-CH3 spacer and the transmembrane domain of human CD4 (DAbR1). The scFv was found to bind irreversibly to yttrium-(*S*)-2-(4-acrylamidobenzyl-)-DOTA (AABD), which could serve as an imaging label when conjugated to an appropriate radioisotope (e.g., using $^{86}$Y for PET imaging). DAbR1 was successfully expressed on lymphocytes and CD19 CAR-Ts. To detect the traceable cells, radiotracer was administered 30 min after T cell injection, with subsequent PET detection showing good contrast 16 h (~1.1 half-lives).[58] While offering a high positron yield, a limitation for longitudinal T cell reporter gene imaging with $^{86}$Y is its long half-life ($\tau$ = 14.7 h), which only permits re-imaging after about 3 days (cf. Observation Time and Interval). Its long positron range also impacts resolution (comparable to $^{124}$I and about 2-fold worse resolution than that of the gold standard, $^{18}$F[180]). These studies demonstrate potentially workable approaches, but they are still in preliminary stages, as none of the reporter genes is fully human/humanized. It remains to be seen whether fully humanized chimeras will become available for T cell imaging. A step ahead in this respect is a reporter gene incorporating the human carcinoembryonic antigen (hCEA) fused to one of various validated human cell surface protein domains to anchor it within the plasma membrane.[53,54] In this case, an antibody or antibody fragment is required to detect hCEA, which is almost exclusively expressed in certain cancers. While tracking agents can be built on the corresponding antibodies/antibody fragments and the whole system is fully human, it is still unsuitable for adoptive T cell therapy tracking if the corresponding cancer or cancer model also expresses hCEA.

Notably, adoptive T cell therapies have been hampered by severe side effects.[13,14] *In vivo* cell tracking offers the significant advantage to detect mistargeting, i.e., unsafe conditions. Imaging of therapeutic mistargeting is dependent on the level of signal at the unintended site, and it therefore varies depending on the disease model, the therapy targeting moieties, and the employed reporter gene. A one-size-fits-all approach to detect mistargeting at different anatomical locations may be feasible

with a foreign reporter (providing there are favorable excretion properties of the corresponding radiotracer), but this would be limited to use in only immunocompromised/immunodeficient disease models. To advance the development of adoptive T cell therapies in syngeneic models, and ultimately for monitoring therapies in patients, the development of host reporters is necessary. Moreover, host reporter gene selection needs to be tailored to the model/condition and the target. Only *in vivo* cell tracking will be able to measure and inform spatiotemporally on therapeutic cell targeting and mistargeting. This requires truly quantitative longitudinal imaging to accurately, reliably, and reproducibly quantify signals from administered cells and background, and thus better implementation of unbiased physical and mathematical analysis methods will need to be used to advance this in the future. Ultimately, these approaches will unlock the ability to intervene earlier in the event of therapeutic mistargeting and thereby avoid the detrimental effects at the off-target site. This intervention could involve utilizing so-called "suicide genes." Some host reporters could be repurposed to act as suicide genes if radiotracers are modified appropriately from labeling/signal generation agent to radiotherapeutic using matched-pair radioisotopes, thus ablating the cell therapy (e.g., NIS, $^{131}I^-$ or $^{188}ReO_4^-$; PSMA, $^{177}$Lu-PSMA-ligand). However, these approaches tend to be slow in their killing response and potentially also induce radiation damage in bystander cells. Instead, dedicated suicide genes have been developed for cell and gene therapies. This includes the inducible caspase-9 (iCaspase9), which is activatable by a cell-permeable dimerizer drug and results in ablation of suicide gene-expressing cells. iCaspase9 shows rapid function (>90% within 30 min[181]) even in the brain,[182] which is crucial in emergency cases. Its main disadvantage is dimerizer drug availability. Thus, alternative approaches have been developed including the following: RQR8 (combined target epitopes from CD34 and CD20 antigens), which binds the widely used pharmaceutical antibody rituximab, resulting in selective deletion of transgene-expressing cells;[183] a ligand-binding and kinase-dead EGFR variant targetable with the pharmaceutical antibody cetuximab;[184] and a rapamycin-activatable iCaspase9.[185] While the latter is suitable for anti-cancer CAR-Ts, it is not suitable for cell therapies relying on rapamycin for their production, e.g., regulatory T cell therapies.[186–188] Both RQR8 and iCaspase9 are already in clinical trials (ClinicalTrials.gov: NCT02808442, NCT02746952, NCT02735083, NCT03939026, NCT03190278, NCT04106076, NCT04142619 and NCT03721068, NCT02849886, and NCT04180059). Nevertheless, the full potential of suicide genes, which enable early destruction of mistargeted therapeutic cells before severe clinical signs become evident, has yet to be fulfilled. This may be achieved in the future by combining detection of early indicators of mistargeting with *in vivo* tracking and quantification of administered cell therapies.

## Cell Tracking in Stem Cell Therapy Development

### *Clinical Tracking of Stem Cell Therapies*

Numerically, so-called "mesenchymal stem cells" make up the highest number of stem cell therapies used in clinical trials to date, although strictly speaking these are often not bona fide stem cell therapies and are more accurately described as a heterogeneous population of multipotent mesenchymal signaling/stromal cells (MSCs), which may contain stem cell subpopulations.[1] In fact, hundreds of clinical trials using these variously defined MSC populations have been performed to date.[1,189] However, in spite of their regenerative potential, MSCs tend to have poor levels of engraftment upon transplant, and it is now thought that their value as cell therapies is to promote self-healing of the damaged tissues through the release of cytokines, chemokines, and growth factors that, in turn, offer the capacity to promote native tissue regeneration and recruit or activate cells at the injury site that encourage regeneration. This contrasts with other therapies using stem/progenitor cells (SCs) or their differentiated progeny, where the goal is to achieve high levels of engraftment post-transplant and often also differentiation, or maturation of the transplanted SC population within its niche. As such, transient cell survival would be a limiting factor to therapeutic benefit. Consequently, it is now recognized that the ability to monitor cells post-transplant via non-invasive *in vivo* tracking could hold the key to improving cell survival and engraftment.

Despite the many potential benefits, only a handful of SC therapy studies utilizing *in vivo* imaging have been performed in the clinic. To our knowledge, these have all adopted a direct cell-labeling approach using either MRI or PET/SPECT modalities to track transplanted cell fate. Autologous neural SCs, MSCs, and hematopoietic SCs have all been directly labeled (Figure 1A) and then monitored *in vivo* to assess neuroregeneration for both trauma injuries and neurodegenerative diseases,[190,191] anti-fibrotic therapeutic effects in advanced liver cirrhosis,[192] or cardiac repair.[193–195] Given the regulatory hurdles associated with genetic engineering of stem cells, avoidance of reporter gene imaging approaches for tracking SC therapies clinically is unsurprising.

### *Reporter Gene-Afforded Pre-clinical Tracking of Stem Cell Therapies*

Comparatively, in the preclinical arena, the potential for reporter genes to enable tracking of SCs isolated from adult tissues, pluripotent SCs (PSCs) such as human embryonic SCs (hESCs) and human induced PSCs (hiPSCs), as well as PSC-differentiated progeny *in vivo* is gaining interest. In Table 3 we list studies using preclinical reporter gene-afforded *in vivo* imaging of SC populations (or their *in vitro*-differentiated progeny) of human origin. Notably, numerous imaging studies using SC populations derived from a range of animal sources have also been reported.[170,196,197] While some reports demonstrate tracking of SC populations isolated from adult tissues, the bulk of studies have focused on developing tools to monitor tumorigenicity of hESCs and hiPSCs *in vivo* or to enable monitoring of survival and engraftment of PSC differentiated progeny. In the case of tumorigenicity, studies monitoring PSC survival and teratoma formation are vital for providing safety assurances prior to use in humans. Undifferentiated PSCs possess tumorigenic potential, so longitudinal *in vivo* imaging allows transplanted differentiated cell populations to be monitored for residual, contaminating PSCs. If PSCs are present in only low numbers, tumor formation may take time to yield a palpable tumor or may be present in deep tissue or at off-target sites, so the nature of monitoring required is incompatible with direct cell labeling

**Table 3. Preclinical studies utilizing reporter gene tracking of stem cell therapies.**

| Cell Therapy | Purpose of Imaging | Reporter Gene (RG) Expressed | Imaging Modality Used | Method of RG transfer | Refs. |
|---|---|---|---|---|---|
| Adult Stem Cells/Tissue Resident Stem Cells | | | | | |
| Human and mouse HSCs | engraftment monitoring | human deoxycytidine kinase with three amino acid substitutions within the active site (hdCK3mut) | PET/CT | lentivirus | 200 |
| Immortalized human neural stem cell line (HB1.F3) | study of epigenetic silencing mechanisms of reporter genes in neural stem cells | hNIS | scintographic imaging | plasmid transfection | 201 |
| Immortalized human bone marrow-derived MSC line | monitoring of MSC homing to tumors and evaluation of their therapeutic potential as a transgenic reporter-expressing cell-based therapy | hNIS | scintographic imaging | plasmid transfection | 202 |
| Human MSCs | monitoring of MSC homing and therapeutic potential in breast cancer | hNIS | SPECT | adenovirus | 203 |
| Human MSCs | tracking of long-term fate and trafficking of MSCs | triple fusion protein: fLuc-mRFP-HSV1-sr39tk | BLI and PET/CT | lentivirus | 204 |
| Human MSCs | understanding MSC fate in tissue repair | mutant of dopamine type 2 receptor (D2R80A) | PET | lentivirus | 205 |
| Human MSCs | evaluating myocardial tracking potential with a PET reporter in small (rat) and large animal studies (swine) | HSV1-sr39tk | PET | adenovirus | 206 |
| hESCs and Their Differentiated Progeny | | | | | |
| Transplanted labeled hESCs/H9 line | tracking immune rejection | fusion protein: fLuc and EGFP | BLI | lentivirus | 207 |
| Human neural stem cells derived from hESCs/H7 line | tracking fate and function of grafted cells in a preclinical stroke model | triple fusion protein: mRFP-fLuc-HSV1-sr39tk | MRI and PET | lentivirus | 208 |
| hESCs | teratoma monitoring after transplant into chick embryos and mice (kidney capsule and muscle of peritoneum) | fLuc | BLI | plasmid transfection | 209 |
| Human ESCs/H9 line | determining application of genome editing for long-term molecular imaging of engrafted stem cells | polycistronic: EGFP/fLuc/hSSTR2 and polycistronic EGFP/fLuc/hNIS | BLI and PET | ZFN targeted at the AAVS1 locus | 210 |
| hESCs/H9 line and one patient derived hiPSC line and hESC-derived ECs and CMs | preclinical monitoring of teratomas and hESC-derived cardiac cells for cardiovascular research/regenerative medicine | triple fusion protein: fLuc-mRFP-HSV1-*tk* | BLI | ZFN targeted at the AAVS1 locus | 211 |
| hESC-derived $CD34^+$ cells/H9 line | tracking engraftment/developmental of hESC-derived HSCs *in vivo* | fLuc | BLI | transfection of DNA transposon system | 212 |
| hESCs/H9 line | safety study: analysis number of contaminating undifferentiated hESCs required to yield a teratoma | fusion protein: fLuc-EGFP | BLI | lentivirus | 198 |
| hESC-derived MSCs | studied the distribution of human MSCs in a rat hindlimb ischemic injury model immediately after transplantation and also analyzed the recipient tissue response to transplanted cells | fLuc | BLI | lentivirus | 213 |

(*Continued on next page*)

**Table 3. *Continued***

| Cell Therapy | Purpose of Imaging | Reporter Gene (RG) Expressed | Imaging Modality Used | Method of RG transfer | Refs. |
|---|---|---|---|---|---|
| hESCs and hESC-derived ECs/H9 line | comparison of MR and bioluminescence modalities for tracking of transplanted cell engraftment and longitudinal monitoring of cell fate | fusion protein: fLuc-EGFP | BLI | lentivirus | 214 |
| hESC-derived neural precursors/H9 line | monitoring of long-term viability and proliferation of hESC-derived neural precursor grafts in the brains of immunodeficient and immunocompetent mice | TGL fusion protein: HSV1-*tk*-EGFP-fLuc | BLI | lentivirus | 215 |
| hESC-derived skeletal myoblasts/H1 and H9 lines | assessment of long-term myoblast engraftment and survival with monitoring for teratoma formation | TGL fusion protein: HSV1-*tk*-EGFP-fLuc | BLI | lentivirus | 216 |
| hESCs/H1 and H9 | monitoring stem cell engraftment and teratoma formation | bicistronic fLuc and GFP and fusion of HSV1-*tk*-GFP | BLI and SPECT/CT | lentivirus | 199 |
| hiPSCs and Their Differentiated Progeny | | | | | |
| hiPSCs differentiated to motor neurons, HLCs, and macrophages | generation of reporter expressing hiPSCs suitable for differentiation into macrophages to track anti-fibrotic potential *in vivo* | ZsGreen | *in vivo* imaging not performed[a] | ZFN targeted at AAVS1 locus | 217 |
| hiPSC-derived HLCs | potential for tracking transplanted HLC populations *in vivo* | hNIS-EGFP fusion | SPECT/CT | lentivirus | 172 |
| hiPSC-derived neural stem/progenitor cells | determining the feasibility of tumor ablation following hiPSC-neural stem/progenitor cell (NS/PC) spinal cord transplantation utilizing immunoregulation | fusion protein Venus-fLuc | BLI | lentivirus | 218 |
| hiPSC-derived endothelial cells | analysis of potential of iPSC-derived ECs to promote perfusion of ischemic tissue in model of peripheral arterial disease | fusion protein: fLuc-EGFP | BLI | lentivirus | 219 |
| hiPSCs | evaluation of transplanted hiPSC survival, engraftment, and distribution of in a pig model of myocardial infarction | bicistronic rat NIS and Venus | SPECT/CT | plasmid transfection | 220 |
| hiPSCs | evaluating systems to purge residual hiPSCs before graft without compromising hematopoietic repopulation capability | fLuc | BLI | lentivirus | 221 |
| hiPSC-derived cardiomyocytes | assessment of relationship between transplanted cell number and engraftment rate in myocardial injury | bicistronic fLuc and GFP | BLI | lentivirus | 222 |

The table illustrates the range of preclinical stem cell therapy studies that have incorporated reporter gene-afforded *in vivo* imaging. Studies are classified based on type of stem cell, with details on the modality and purpose of *in vivo* tracking used as well as the reporter gene and method of construct integration. HSC, hematopoietic stem cell; hESC, human embryonic stem cell; hiPSC, human induced pluripotent stem cell; RG, reporter gene; EC, endothelial cell; CM, cardiomyocyte; HLC, hepatocyte-like cell; ZFN, zinc finger nuclease; fLuc, firefly luciferase; mRFP, monomeric red fluorescence protein; HSV1-*tk*, herpes simplex virus type 1 thymidine kinase; HSV1-sr39tk, truncated HSV1-sr39 thymidine kinase; hNIS, human sodium iodide symporter; hSSTR2, human somatostatin receptor 2; BLI, bioluminescence imaging.
[a]Cited as a tool with the potential for macrophage *in vivo* tracking in the future.

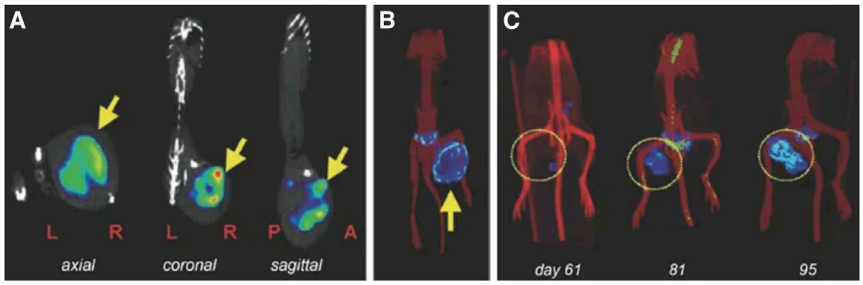


**Figure 6. Example of Reporter Gene Integration to Enable Non-invasive Monitoring of Stem Cell-Mediated Teratoma Formation by *In Vivo* Imaging**

Human ESCs were lentivirally modified to express the HSV1-*tk* radionuclide reporter gene fused to enhanced GFP, and 2–5 × $10^6$ reporter expressing hESCs were injected intramuscularly and tracked *in vivo* by whole-body SPECT/CT imaging. Yellow arrows/rings indicate tumors. (A and B) Representative planar (A) γ and (B) SPECT/CT images of tumors derived in an animal scanned 87 days after tumor inoculation (when a palpable tumor was detected). The radiotracer [$^{125}$I]FIAU was intravenously (i.v.) administered and the animal was scanned 24 h later. (C) Longitudinal SPECT/CT imaging of a different SCID (severe combined immunodeficiency)-beige mouse harboring a teratoma from reporter-expressing hESCs. This mouse was serially imaged at the indicated time points post inoculation. All data were quantitatively analyzed in the study. For details the reader is referred to the original work[199]. [Figure reproduced with minor modification from the cited work.]

approaches. Reporter gene imaging, however, can offer cell tracking over longer time frames, and the possibility to determine the minimum number of PSCs that would go on to form a tumor, allowing differentiation purity thresholds to be set (Figure 6).[198,199]

For cell populations differentiated from PSCs, aside from monitoring tumorigenicity, the goal of *in vivo* imaging is typically to assess engraftment and survival post-transplant. While direct cell labeling can inform on immediate survival post-transplant, reporter gene imaging is again needed to assess the long-term survival of these therapies. At the preclinical level such monitoring can aid in important therapeutic decisions such as site of transplant (ectopic site or within appropriate tissue niche), required cell numbers to enable longitudinal cell survival, level of engraftment, and whether factors such as transplantation of organoids, cell scaffolds, or use of a supporting extracellular matrix would be necessary, all while using appropriate animal models for the intended patient population.

While PSC-derived therapies are costly to produce, they have already entered early clinical trials,[223] and as their use for treating a greater range of injuries and diseases comes ever closer to clinical reality, reporter gene studies become increasingly important. Most early PSC therapy-tracking studies incorporated the reporter cassette via lentiviral transduction and utilized the firefly luciferase (fLuc) reporter gene to enable bioluminescence imaging (BLI), often with an additional reporter co-expressed for streamlining preclinical experimentation, e.g., a fluorescent protein to simplify cell generation (Table 3). Use of BLI is due to its exquisite sensitivity at low running and investment cost, despite sacrificing 3D information for 2D-projected images. BLI has been shown to address narrow questions relating to graft survival adequately. Assessment of therapy relocalization *in vivo* is also feasible by BLI, albeit at the expense of identification of the off-target site, as BLI does not provide true 3D tomographic information. Radionuclide reporter gene imaging could help overcome this limitation, but it has been employed only by a few studies using human PSCs to date.[172,199,206,220] Additionally, while studies using lentiviral-mediated reporter expression have mostly demonstrated stable reporter expression following both differentiation and PSC expansion, the risk of epigenetic silencing and viral integration at unwanted genomic sites remains. Consequently, gene editing as a means for incorporation of transgenes into safe harbor loci has been widely employed for *in vitro* research.[224] While initially focused on fluorescent proteins and microscopy, this approach is now emerging for *in vivo* imaging-compatible reporter genes, including those required for cell tracking by BLI and radionuclide imaging. Exploiting the adeno-associated virus integration site 1 (AAVS1) locus and using zinc finger nucleases (ZFNs) for stable reporter gene expression have been observed in both hESCs and differentiated cells.[211,210]

A final point to consider is that of the studies tracking hESCs there has been a significant focus on use of the earliest lines derived at the University of Wisconsin, i.e., H1, H7, and H9.[225] While easily commercially available, similar to hiPSCs, these lines have widely been reported to be prone to acquiring significant genomic abnormalities following extended periods of propagation, dependent on culture conditions.[226] Unlike hESCs, however, systematically characterized allogeneic hiPSC banks are in production across the globe to enable high levels of immunocompatibility with the population ahead of wider clinical application of regenerative medicines, and thus hiPSC tracking studies may prove to be the most translationally relevant stem cell tracking technology moving forward.[227]

## Considerations for Clinical Application or Reporter Gene Imaging and Outlook

Cell therapies can be classified as either (1) not in need of genetic engineering for efficacy (e.g., all currently approved stem cell therapies, tumor infiltrating lymphocytes, γδ T cells), or (2) fundamentally requiring genetic engineering for efficacy (e.g., CAR-Ts, TCR-Ts). For *in vivo* tracking of the first group, the choice between direct and indirect cell labeling depends on the precise research question, practicalities, and of course whether clinical translation of the tracking methodology is envisaged and for what purpose. Implementing genetic engineering for the sole purpose of clinical long-term cell tracking currently appears out of reach for these therapies, as it adds a significant regulatory burden and potential risk depending on the gene transfer technique used, all of which are difficult to justify. Consequently, recently developed direct cell-tracking approaches (e.g., based on

[$^{89}$Zr]Zr-oxine and matched with PET imaging[228–230]) are promising tools despite their obvious limitations caused by the cell-labeling methodology itself (label efflux, label dilution, complex dosimetry, limited observation times). The situation is likely to improve through the development of total-body PET, which has been reported to be 40-fold more sensitive than conventional PET.[231] This sensitivity advantage could either be invested into faster PET scanning, scanning with reduced radioactivity, or both of the above. Future *in vivo* cell tracking studies using total-body PET technology will reveal to what extent this sensitivity advantage can be used to extend the tracking time of directly labeled cells.

For cell-based immunotherapies that require genetic engineering, an immunocompatible host reporter gene can be implemented without adding to the regulatory burden. Indirect cell labeling is clearly advantageous over direct cell labeling in such cases, as it enables longer-term monitoring, reflects cell proliferation and viability, and avoids complex dosimetry considerations during cell labeling. Precise radiobiological characterization of the effects of radiotracer uptake and decay within immune cells and stem cells has not yet been fully elucidated. However, the use of short-lived radioisotopes, particularly for PET-afforded reporter gene imaging, provides a clear dose reduction compared to any form of long-term cell tracking using direct radioisotope labeling approaches. Genetic engineering technologies have steadily advanced and include viral and non-viral delivery methods as well as site-specific integration via gene editing approaches (Figure 3C). While new vectors inherently trigger safety evaluations and thus are expensive to develop, there has still been significant progress in this domain in recent years,[232,233] with ready-to-use platforms for clinical use available.[7,12] Crucially, reporter genes must be co-delivered either in the same or a separate vector with therapeutic genes, for example the CAR. This has previously been demonstrated by rendering CAR-Ts traceable by SPECT or PET[29,174] and is fundamentally the same concept as is exploited for adding other therapy-relevant payloads such as CAR-dependent expression of immune checkpoint antibodies or cytokines (cf. different CAR-T generations and armored CARs[234]). If activity of therapeutic cells is envisaged, a system with two reports, an inducible one and a beacon reporter, can be employed, which in principle could also operate for radionuclide reporters. However, in the context of clinical translation, such an approach would add a high level of complexity, duplicating effort, cost, and likely resulting in logistically more convoluted reporter gene imaging. This is because it would require a concurrent supply of two radiotracers that can either be discriminated temporally through different administration/imaging time windows or discriminated by simultaneous dual-isotope imaging approaches (e.g., afforded by SPECT or dual-isotope PET[121–123]). Currently, such methods are not routinely available either preclinically or clinically. More research is needed to devise new smart reporter systems compatible with radionuclide imaging that can also report on environmental changes, for example CAR T cell activity, without the need for a second reporter for normalization. Another crucial aspect for clinical reporter gene imaging is the range of suitable labeling agents available. A scenario where labeling agents are already clinically approved, non-toxic, and widely and easily accessible (e.g., radiotracers such as $^{99m}TcO_4^-$ and [$^{18}$F]$BF_4^-$ for NIS or [$^{68}$Ga]Ga-PSMA-ligands for PSMA) is obviously advantageous compared to the development of a reporter gene that would additionally require lengthy radiopharmaceutical development and subsequent regulatory approval. It is unlikely that a one-size-fits-all approach across varying cell therapies and disease conditions will ever be available. For example, oncology cancers differ in their anatomical location, and hence involving only one immunocompatible host reporter gene/radiotracer pair for cell therapy tracking is very unlikely to meet all requirements. More likely, various cancers at different anatomical sites with varying endogenous host reporter expression levels will be targeted by genetically engineered cell-based immunotherapies, where the target as well as the host reporter will be somewhat tailored to the individual patient.

All of the above concepts can be extrapolated to cell therapies intended to treat other conditions, such as those in the fields of regenerative medicine,[235] transplantation,[187,236] diabetes type I,[237,238] multiple sclerosis,[239] and infectious diseases.[240] Undoubtedly, to drive reporter gene imaging closer to future routine clinical application, more research into optimizing existing and developing new host reporter/labeling agent pairs is warranted. This will offer the most flexible toolkit to render cell therapies traceable *in vivo* with the best contrast and optimal readout, in a truly quantitative manner.

## AUTHOR CONTRIBUTIONS

G.O.F. contributed the article concept; M.I. and G.O.F. compiled the figures; C.A.-H., M.I., A.S., and G.O.F. wrote sections of the manuscript. All authors contributed to literature searches, manuscript revision, and read and approved the submitted version.

## CONFLICTS OF INTEREST

The authors declare no competing interests.

## ACKNOWLEDGMENTS

The authors received support from Guy's and St Thomas' Charity (PhD studentship to C.A.-H.), EPSRC and GE Healthcare (PhD studentship to M.I.), MRC (PhD studentship to A.S.), and Cancer Research UK via a Multidisciplinary Project Award (C48390/A21153) to G.O.F. Furthermore, the authors are supported by the King's College London and UCL Comprehensive Cancer Imaging Centre, funded by Cancer Research UK and EPSRC; the National Institute for Health Research (NIHR) Biomedical Research Centre based at Guy's and St Thomas' NHS Foundation Trust and King's College London; and the Wellcome/EPSRC Centre for Medical Engineering at King's College London (WT 203148/Z/16/Z). Institutional Open Access funds to support article publication were also received. The views expressed are those of the authors and not necessarily those of the NHS, the NIHR, or the DoH. Aspects of Figures 1, 3, and 4 were created with Biorender.com.

## REFERENCES


1. Caplan, A.I. (2017). Mesenchymal stem cells: time to change the name! Stem Cells Transl. Med. *6*, 1445–1451.
2. Heathman, T.R., Nienow, A.W., McCall, M.J., Coopman, K., Kara, B., and Hewitt, C.J. (2015). The translation of cell-based therapies: clinical landscape and manufacturing challenges. Regen. Med. *10*, 49–64.
3. BioInformant (2019). BioInformant cell therapy industry database, https://bioinformant.com/product/cell-therapy-industry-database/.
4. Society, A.C. (1991). Unproven methods of cancer management. Fresh cell therapy. CA Cancer J. Clin. *41*, 126–128.
5. Thomas, E.D., Lochte, H.L., Jr., Lu, W.C., and Ferrebee, J.W. (1957). Intravenous infusion of bone marrow in patients receiving radiation and chemotherapy. N. Engl. J. Med. *257*, 491–496.
6. Appelbaum, F.R. (2007). Hematopoietic-cell transplantation at 50. N. Engl. J. Med. *357*, 1472–1475.
7. Neelapu, S.S., Locke, F.L., Bartlett, N.L., Lekakis, L.J., Miklos, D.B., Jacobson, C.A., Braunschweig, I., Oluwole, O.O., Siddiqi, T., Lin, Y., et al. (2017). Axicabtagene ciloleucel CAR T-cell therapy in refractory large B-cell lymphoma. N. Engl. J. Med. *377*, 2531–2544.
8. Schuster, S.J., Bishop, M.R., Tam, C.S., Waller, E.K., Borchmann, P., McGuirk, J.P., Jäger, U., Jaglowski, S., Andreadis, C., Westin, J.R., et al.; JULIET Investigators (2019). Tisagenlecleucel in adult relapsed or refractory diffuse large B-cell lymphoma. N. Engl. J. Med. *380*, 45–56.
9. Schuster, S.J., Svoboda, J., Chong, E.A., Nasta, S.D., Mato, A.R., Anak, Ö., Brogdon, J.L., Pruteanu-Malinici, I., Bhoj, V., Landsburg, D., et al. (2017). Chimeric antigen receptor T cells in refractory B-cell lymphomas. N. Engl. J. Med. *377*, 2545–2554.
10. US Food and DrugAdministration (2017). FDA approves CAR-T cell therapy to treat adults with certain types of large B-cell lymphoma (N/A), https://www.fda.gov/NewsEvents/Newsroom/PressAnnouncements/ucm581216.htm.
11. US Food and DrugAdministration (2017). FDA approval brings first gene therapy to the United States (N/A), https://www.fda.gov/news-events/press-announcements/fda-approval-brings-first-gene-therapy-united-states.
12. Maude, S.L., Laetsch, T.W., Buechner, J., Rives, S., Boyer, M., Bittencourt, H., Bader, P., Verneris, M.R., Stefanski, H.E., Myers, G.D., et al. (2018). Tisagenlecleucel in children and young adults with B-cell lymphoblastic leukemia. N. Engl. J. Med. *378*, 439–448.
13. Linette, G.P., Stadtmauer, E.A., Maus, M.V., Rapoport, A.P., Levine, B.L., Emery, L., Litzky, L., Bagg, A., Carreno, B.M., Cimino, P.J., et al. (2013). Cardiovascular toxicity and titin cross-reactivity of affinity-enhanced T cells in myeloma and melanoma. Blood *122*, 863–871.
14. Saudemont, A., Jespers, L., and Clay, T. (2018). Current status of gene engineering cell therapeutics. Front. Immunol. *9*, 153.
15. Fruhwirth, G.O., Kneilling, M., de Vries, I.J.M., Weigelin, B., Srinivas, M., and Aarntzen, E.H.J.G. (2018). The potential of in vivo imaging for optimization of molecular and cellular anti-cancer immunotherapies. Mol. Imaging Biol. *20*, 696–704.
16. Krekorian, M., Fruhwirth, G.O., Srinivas, M., Figdor, C.G., Heskamp, S., Witney, T.H., and Aarntzen, E.H.J.G. (2019). Imaging of T-cells and their responses during anti-cancer immunotherapy. Theranostics *9*, 7924–7947.
17. Volpe, A., Kurtys, E., and Fruhwirth, G.O. (2018). Cousins at work: how combining medical with optical imaging enhances in vivo cell tracking. Int. J. Biochem. Cell Biol. *102*, 40–50.
18. Jones, B.S., Lamb, L.S., Goldman, F., and Di Stasi, A. (2014). Improving the safety of cell therapy products by suicide gene transfer. Front. Pharmacol. *5*, 254.
19. Abou-El-Enein, M., Bauer, G., Reinke, P., Renner, M., and Schneider, C.K. (2014). A roadmap toward clinical translation of genetically-modified stem cells for treatment of HIV. Trends Mol. Med. *20*, 632–642.
20. Ashmore-Harris, C., and Fruhwirth, G.O. (2020). The clinical potential of gene editing as a tool to engineer cell-based therapeutics. Clin. Transl. Med. *9*, 15.
21. Kircher, M.F., Gambhir, S.S., and Grimm, J. (2011). Noninvasive cell-tracking methods. Nat. Rev. Clin. Oncol. *8*, 677–688.
22. Portulano, C., Paroder-Belenitsky, M., and Carrasco, N. (2014). The $Na^+/I^-$ symporter (NIS): mechanism and medical impact. Endocr. Rev. *35*, 106–149.
23. Kogai, T., and Brent, G.A. (2012). The sodium iodide symporter (NIS): regulation and approaches to targeting for cancer therapeutics. Pharmacol. Ther. *135*, 355–370.
24. Oliveira, J.M., Gomes, C., Faria, D.B., Vieira, T.S., Silva, F.A., Vale, J., and Pimentel, F.L. (2017). $^{68}$Ga-prostate-specific membrane antigen positron emission tomography/computed tomography for prostate cancer imaging: a narrative literature review. World J. Nucl. Med. *16*, 3–7.
25. Perera, M., Papa, N., Christidis, D., Wetherell, D., Hofman, M.S., Murphy, D.G., Bolton, D., and Lawrentschuk, N. (2016). Sensitivity, specificity, and predictors of positive $^{68}$Ga-prostate-specific membrane antigen positron emission tomography in advanced prostate cancer: a systematic review and meta-analysis. Eur. Urol. *70*, 926–937.
26. Tiernan, J.P., Perry, S.L., Verghese, E.T., West, N.P., Yeluri, S., Jayne, D.G., and Hughes, T.A. (2013). Carcinoembryonic antigen is the preferred biomarker for in vivo colorectal cancer targeting. Br. J. Cancer *108*, 662–667.
27. Tsao, H., Chin, L., Garraway, L.A., and Fisher, D.E. (2012). Melanoma: from mutations to medicine. Genes Dev. *26*, 1131–1155.
28. Castanares, M.A., Mukherjee, A., Chowdhury, W.H., Liu, M., Chen, Y., Mease, R.C., Wang, Y., Rodriguez, R., Lupold, S.E., and Pomper, M.G. (2014). Evaluation of prostate-specific membrane antigen as an imaging reporter. J. Nucl. Med. *55*, 805–811.
29. Minn, I., Huss, D.J., Ahn, H.H., Chinn, T.M., Park, A., Jones, J., Brummet, M., Rowe, S.P., Sysa-Shah, P., Du, Y., et al. (2019). Imaging CAR T cell therapy with PSMA-targeted positron emission tomography. Sci. Adv. *5*, eaaw5096.
30. Qin, C., Lan, X., He, J., Xia, X., Tian, Y., Pei, Z., Yuan, H., and Zhang, Y. (2013). An in vitro and in vivo evaluation of a reporter gene/probe system hERL/$^{18}$F-FES. PLoS ONE *8*, e61911.
31. Urabe, K., Aroca, P., Tsukamoto, K., Mascagna, D., Palumbo, A., Prota, G., and Hearing, V.J. (1994). The inherent cytotoxicity of melanin precursors: a revision. Biochim. Biophys. Acta *1221*, 272–278.
32. Lee, J.T., Zhang, H., Moroz, M.A., Likar, Y., Shenker, L., Sumzin, N., Lobo, J., Zurita, J., Collins, J., van Dam, R.M., and Ponomarev, V. (2017). Comparative analysis of human nucleoside kinase-based reporter systems for PET imaging. Mol. Imaging Biol. *19*, 100–108.
33. Volpe, A., Man, F., Lim, L., Khoshnevisan, A., Blower, J., Blower, P.J., and Fruhwirth, G.O. (2018). Radionuclide-fluorescence reporter gene imaging to track tumor progression in rodent tumor models. J. Vis. Exp. *133*, e57088.
34. Khoshnevisan, A., Chuamsaamarkkee, K., Boudjemeline, M., Jackson, A., Smith, G.E., Gee, A.D., Fruhwirth, G.O., and Blower, P.J. (2017). $^{18}$F-fluorosulfate for PET imaging of the sodium-iodide symporter: synthesis and biologic evaluation in vitro and in vivo. J. Nucl. Med. *58*, 156–161.
35. Jiang, H., Bansal, A., Goyal, R., Peng, K.W., Russell, S.J., and DeGrado, T.R. (2018). Synthesis and evaluation of $^{18}$F-hexafluorophosphate as a novel PET probe for imaging of sodium/iodide symporter in a murine C6-glioma tumor model. Bioorg. Med. Chem. *26*, 225–231.
36. Jauregui-Osoro, M., Sunassee, K., Weeks, A.J., Berry, D.J., Paul, R.L., Cleij, M., Banga, J.P., O'Doherty, M.J., Marsden, P.K., Clarke, S.E., et al. (2010). Synthesis and biological evaluation of [$^{18}$F]tetrafluoroborate: a PET imaging agent for thyroid disease and reporter gene imaging of the sodium/iodide symporter. Eur. J. Nucl. Med. Mol. Imaging *37*, 2108–2116.
37. Dai, G., Levy, O., and Carrasco, N. (1996). Cloning and characterization of the thyroid iodide transporter. Nature *379*, 458–460.
38. Khoshnevisan, A., Jauregui-Osoro, M., Shaw, K., Torres, J.B., Young, J.D., Ramakrishnan, N.K., Jackson, A., Smith, G.E., Gee, A.D., and Blower, P.J. (2016). [$^{18}$F]tetrafluoroborate as a PET tracer for the sodium/iodide symporter: the importance of specific activity. EJNMMI Res. *6*, 34.
39. Moroz, M.A., Serganova, I., Zanzonico, P., Ageyeva, L., Beresten, T., Dyomina, E., Burnazi, E., Finn, R.D., Doubrovin, M., and Blasberg, R.G. (2007). Imaging hNET reporter gene expression with $^{124}$I-MIBG. J. Nucl. Med. *48*, 827–836.
40. Pulé, M., Badar, A., Kiru, L., Lythgoe, M., and Peters, A. (2017). Detecting a therapeutic cell. US patent application publication 20170056534 A1, filed August 25, 2015, and published March 2, 2017.

41. Haywood, T., Beinat, C., Gowrishankar, G., Patel, C.B., Alam, I.S., Murty, S., and Gambhir, S.S. (2019). Positron emission tomography reporter gene strategy for use in the central nervous system. Proc. Natl. Acad. Sci. USA *116*, 11402–11407.

42. Ponomarev, V., Doubrovin, M., Shavrin, A., Serganova, I., Beresten, T., Ageyeva, L., Cai, C., Balatoni, J., Alauddin, M., and Gelovani, J. (2007). A human-derived reporter gene for noninvasive imaging in humans: mitochondrial thymidine kinase type 2. J. Nucl. Med. *48*, 819–826.

43. Likar, Y., Zurita, J., Dobrenkov, K., Shenker, L., Cai, S., Neschadim, A., Medin, J.A., Sadelain, M., Hricak, H., and Ponomarev, V. (2010). A new pyrimidine-specific reporter gene: a mutated human deoxycytidine kinase suitable for PET during treatment with acycloguanosine-based cytotoxic drugs. J. Nucl. Med. *51*, 1395–1403.

44. Rogers, B.E., McLean, S.F., Kirkman, R.L., Della Manna, D., Bright, S.J., Olsen, C.C., Myracle, A.D., Mayo, M.S., Curiel, D.T., and Buchsbaum, D.J. (1999). In vivo localization of [$^{111}$In]-DTPA-D-Phe1-octreotide to human ovarian tumor xenografts induced to express the somatostatin receptor subtype 2 using an adenoviral vector. Clin. Cancer Res. *5*, 383–393.

45. Chaudhuri, T.R., Rogers, B.E., Buchsbaum, D.J., Mountz, J.M., and Zinn, K.R. (2001). A noninvasive reporter system to image adenoviral-mediated gene transfer to ovarian cancer xenografts. Gynecol. Oncol. *83*, 432–438.

46. Zinn, K.R., Buchsbaum, D., Chaudhuri, T.R., Mountz, J.M., Grizzle, W.E., Krasnykh, V.N., Curiel, D.T., and Rogers, B.E. (2000). Simultaneous in vivo imaging of thymidine kinase and somatostatin receptor expression after gene transfer with an adenoviral vector encoding both genes. Mol. Ther. *1* (*Suppl*), S44.

47. Rogers, B.E., Zinn, K.R., and Buchsbaum, D.J. (2000). Gene transfer strategies for improving radiolabeled peptide imaging and therapy. Q. J. Nucl. Med. *44*, 208–223.

48. MacLaren, D.C., Gambhir, S.S., Satyamurthy, N., Barrio, J.R., Sharfstein, S., Toyokuni, T., Wu, L., Berk, A.J., Cherry, S.R., Phelps, M.E., and Herschman, H.R. (1999). Repetitive, non-invasive imaging of the dopamine D2 receptor as a reporter gene in living animals. Gene Ther. *6*, 785–791.

49. Liang, Q., Satyamurthy, N., Barrio, J.R., Toyokuni, T., Phelps, M.P., Gambhir, S.S., and Herschman, H.R. (2001). Noninvasive, quantitative imaging in living animals of a mutant dopamine D2 receptor reporter gene in which ligand binding is uncoupled from signal transduction. Gene Ther. *8*, 1490–1498.

50. Satyamurthy, N., Barrio, J.R., Bida, G.T., Huang, S.C., Mazziotta, J.C., and Phelps, M.E. (1990). 3-(2′-[$^{18}$F]fluoroethyl)spiperone, a potent dopamine antagonist: synthesis, structural analysis and in-vivo utilization in humans. Int. J. Rad. Appl. Instrum. [A] *41*, 113–129.

51. Hwang, D.W., Kang, J.H., Chang, Y.S., Jeong, J.M., Chung, J.K., Lee, M.C., Kim, S., and Lee, D.S. (2007). Development of a dual membrane protein reporter system using sodium iodide symporter and mutant dopamine D2 receptor transgenes. J. Nucl. Med. *48*, 588–595.

52. Weissleder, R., Moore, A., Mahmood, U., Bhorade, R., Benveniste, H., Chiocca, E.A., and Basilion, J.P. (2000). In vivo magnetic resonance imaging of transgene expression. Nat. Med. *6*, 351–355.

53. Barat, B., Kenanova, V.E., Olafsen, T., and Wu, A.M. (2011). Evaluation of two internalizing carcinoembryonic antigen reporter genes for molecular imaging. Mol. Imaging Biol. *13*, 526–535.

54. Kenanova, V., Barat, B., Olafsen, T., Chatziioannou, A., Herschman, H.R., Braun, J., and Wu, A.M. (2009). Recombinant carcinoembryonic antigen as a reporter gene for molecular imaging. Eur. J. Nucl. Med. Mol. Imaging *36*, 104–114.

55. Hammarström, S. (1999). The carcinoembryonic antigen (CEA) family: structures, suggested functions and expression in normal and malignant tissues. Semin. Cancer Biol. *9*, 67–81.

56. Hong, H., Sun, J., and Cai, W. (2008). Radionuclide-based cancer imaging targeting the carcinoembryonic antigen. Biomark. Insights *3*, 435–451.

57. Girgis, M.D., Olafsen, T., Kenanova, V., McCabe, K.E., Wu, A.M., and Tomlinson, J.S. (2011). Targeting CEA in pancreas cancer xenografts with a mutated scFv-Fc antibody fragment. EJNMMI Res. *1*, 24.

58. Wei, L.H., Olafsen, T., Radu, C., Hildebrandt, I.J., McCoy, M.R., Phelps, M.E., Meares, C., Wu, A.M., Czernin, J., and Weber, W.A. (2008). Engineered antibody fragments with infinite affinity as reporter genes for PET imaging. J. Nucl. Med. *49*, 1828–1835.

59. Chuang, K.H., Wang, H.E., Cheng, T.C., Tzou, S.C., Tseng, W.L., Hung, W.C., Tai, M.H., Chang, T.K., Roffler, S.R., and Cheng, T.L. (2010). Development of a universal anti-polyethylene glycol reporter gene for noninvasive imaging of PEGylated probes. J. Nucl. Med. *51*, 933–941.

60. Cohen, B., Dafni, H., Meir, G., Harmelin, A., and Neeman, M. (2005). Ferritin as an endogenous MRI reporter for noninvasive imaging of gene expression in C6 glioma tumors. Neoplasia *7*, 109–117.

61. Genove, G., DeMarco, U., Xu, H., Goins, W.F., and Ahrens, E.T. (2005). A new transgene reporter for in vivo magnetic resonance imaging. Nat. Med. *11*, 450–454.

62. Louie, A.Y., Hüber, M.M., Ahrens, E.T., Rothbächer, U., Moats, R., Jacobs, R.E., Fraser, S.E., and Meade, T.J. (2000). In vivo visualization of gene expression using magnetic resonance imaging. Nat. Biotechnol. *18*, 321–325.

63. Liu, L., and Mason, R.P. (2010). Imaging β-galactosidase activity in human tumor xenografts and transgenic mice using a chemiluminescent substrate. PLoS ONE *5*, e12024.

64. Li, L., Zemp, R.J., Lungu, G., Stoica, G., and Wang, L.V. (2007). Photoacoustic imaging of lacZ gene expression in vivo. J. Biomed. Opt. *12*, 020504.

65. Guo, Y., Hui, C.-Y., Liu, L., Zheng, H.-Q., and Wu, H.-M. (2019). Improved monitoring of low-level transcription in *Escherichia coli* by a β-galactosidase α-complementation system. Front. Microbiol. *10*, 1454.

66. Krueger, M.A., Cotton, J.M., Zhou, B., Wolter, K., Schwenck, J., Kuehn, A., Fuchs, K., Maurer, A., La Fougere, C., Zender, L., et al. (2019). [$^{18}$F]FPyGal: a novel β-galactosidase specific PET tracer for in vivo imaging of tumor senescence. Cancer Res. *79* (13 Suppl), 1146.

67. Fowler, A.V., and Zabin, I. (1977). The amino acid sequence of beta-galactosidase of Escherichia coli. Proc. Natl. Acad. Sci. USA *74*, 1507–1510.

68. Green, O., Gnaim, S., Blau, R., Eldar-Boock, A., Satchi-Fainaro, R., and Shabat, D. (2017). Near-infrared dioxetane luminophores with direct chemiluminescence emission mode. J. Am. Chem. Soc. *139*, 13243–13248.

69. Sellmyer, M.A., Richman, S.A., Lohith, K., Hou, C., Weng, C.-C., Mach, R.H., O'Connor, R.S., Milone, M.C., and Farwell, M.D. (2020). Imaging CAR T cell trafficking with eDHFR as a PET reporter gene. Mol. Ther. *28*, 42–51.

70. Sellmyer, M.A., Lee, I., Hou, C., Lieberman, B.P., Zeng, C., Mankoff, D.A., and Mach, R.H. (2017). Quantitative PET reporter gene imaging with [$^{11}$C]trimethoprim. Mol. Ther. *25*, 120–126.

71. Tjuvajev, J.G., Stockhammer, G., Desai, R., Uehara, H., Watanabe, K., Gansbacher, B., and Blasberg, R.G. (1995). Imaging the expression of transfected genes in vivo. Cancer Res. *55*, 6126–6132.

72. Jang, S.J., Kang, J.H., Kim, K.I., Lee, T.S., Lee, Y.J., Lee, K.C., Woo, K.S., Chung, W.S., Kwon, H.C., Ryu, C.J., et al. (2010). Application of bioluminescence imaging to therapeutic intervention of herpes simplex virus type I—thymidine kinase/ganciclovir in glioma. Cancer Lett. *297*, 84–90.

73. Jang, S.J., Lee, Y.J., Lim, S., Kim, K.I., Lee, K.C., An, G.I., Lee, T.S., Cheon, G.J., Lim, S.M., and Kang, J.H. (2012). Imaging of a localized bacterial infection with endogenous thymidine kinase using radioisotope-labeled nucleosides. Int. J. Med. Microbiol. *302*, 101–107.

74. Park, J.H., Kim, K.I., Lee, K.C., Lee, Y.J., Lee, T.S., Chung, W.S., Lim, S.M., and Kang, J.H. (2015). Assessment of α-fetoprotein targeted HSV1-*tk* expression in hepatocellular carcinoma with in vivo imaging. Cancer Biother. Radiopharm. *30*, 8–15.

75. Seo, M.-J., Park, J.H., Lee, K.C., Lee, Y.J., Lee, T.S., Choi, T.H., et al. (2020). Small animal PET imaging of hTERT RNA-targeted HSV1-tk gene expression with *trans*-splicing ribozyme. Cancer Biother. Radiopharm. *35*, 26–32.

76. Uchibori, R., Teruya, T., Ido, H., Ohmine, K., Sehara, Y., Urabe, M., Mizukami, H., Mineno, J., and Ozawa, K. (2018). Functional analysis of an inducible promoter driven by activation signals from a chimeric antigen receptor. Mol. Ther. Oncolytics *12*, 16–25.

77. Nakajima, Y., Yamazaki, T., Nishii, S., Noguchi, T., Hoshino, H., Niwa, K., Viviani, V.R., and Ohmiya, Y. (2010). Enhanced beetle luciferase for high-resolution bioluminescence imaging. PLoS ONE *5*, e10011.

78. Nishiguchi, T., Yamada, T., Nasu, Y., Ito, M., Yoshimura, H., and Ozawa, T. (2015). Development of red-shifted mutants derived from luciferase of Brazilian click beetle Pyrearinus termitilluminans. J. Biomed. Opt. *20*, 101205.

79. Morikawa, K., Nakamura, K., Suyama, Y., Yamamoto, K., Fukuoka, K., Yagi, S., Shirayoshi, Y., Ohbayashi, T., and Hisatome, I. (2019). Novel dual-reporter transgenic rodents enable cell tracking in animal models of stem cell transplantation. Biochem. Biophys. Rep. *18*, 100645.

80. Mezzanotte, L., van 't Root, M., Karatas, H., Goun, E.A., and Löwik, C.W.G.M. (2017). In vivo molecular bioluminescence imaging: new tools and applications. Trends Biotechnol. *35*, 640–652.

81. Weihs, F., and Dacres, H. (2019). Red-shifted bioluminescence Resonance Energy Transfer: Improved tools and materials for analytical in vivo approaches. Trends Analyt. Chem. *116*, 61–73.

82. Aswendt, M., Vogel, S., Schäfer, C., Jathoul, A., Pule, M., and Hoehn, M. (2019). Quantitative in vivo dual-color bioluminescence imaging in the mouse brain. Neurophotonics *6*, 025006.

83. Inoue, Y., Sheng, F., Kiryu, S., Watanabe, M., Ratanakanit, H., Izawa, K., Tojo, A., and Ohtomo, K. (2011). Gaussia luciferase for bioluminescence tumor monitoring in comparison with firefly luciferase. Mol. Imaging *10*, 377–385.

84. Tannous, B.A. (2009). *Gaussia* luciferase reporter assay for monitoring biological processes in culture and in vivo. Nat. Protoc. *4*, 582–591.

85. Hunt, E.A., Moutsiopoulou, A., Ioannou, S., Ahern, K., Woodward, K., Dikici, E., Daunert, S., and Deo, S.K. (2016). Truncated variants of *Gaussia* luciferase with tyrosine linker for site-specific bioconjugate applications. Sci. Rep. *6*, 26814.

86. Zhang, Y., Wang, C., Gao, N., Zhang, X., Yu, X., Xu, J., and Gao, F. (2019). Determination of neutralization activities by a new versatile assay using an HIV-1 genome carrying the Gaussia luciferase gene. J. Virol. Methods *267*, 22–28.

87. Mezzanotte, L., An, N., Mol, I.M., Löwik, C.W., and Kaijzel, E.L. (2014). A new multicolor bioluminescence imaging platform to investigate NF-κB activity and apoptosis in human breast cancer cells. PLoS ONE *9*, e85550.

88. Hall, M.P., Unch, J., Binkowski, B.F., Valley, M.P., Butler, B.L., Wood, M.G., Otto, P., Zimmerman, K., Vidugiris, G., Machleidt, T., et al. (2012). Engineered luciferase reporter from a deep sea shrimp utilizing a novel imidazopyrazinone substrate. ACS Chem. Biol. *7*, 1848–1857.

89. La Barbera, G., Capriotti, A.L., Michelini, E., Piovesana, S., Calabretta, M.M., Zenezini Chiozzi, R., Roda, A., and Laganà, A. (2017). Proteomic analysis and bioluminescent reporter gene assays to investigate effects of simulated microgravity on Caco-2 cells. Proteomics *17*, 1700081.

90. Schaub, F.X., Reza, M.S., Flaveny, C.A., Li, W., Musicant, A.M., Hoxha, S., Guo, M., Cleveland, J.L., and Amelio, A.L. (2015). Fluorophore-NanoLuc BRET reporters enable sensitive in vivo optical imaging and flow cytometry for monitoring tumorigenesis. Cancer Res. *75*, 5023–5033.

91. Germain-Genevois, C., Garandeau, O., and Couillaud, F. (2016). Detection of brain tumors and systemic metastases using NanoLuc and Fluc for dual reporter imaging. Mol. Imaging Biol. *18*, 62–69.

92. Lorenz, W.W., McCann, R.O., Longiaru, M., and Cormier, M.J. (1991). Isolation and expression of a cDNA encoding Renilla reniformis luciferase. Proc. Natl. Acad. Sci. USA *88*, 4438–4442.

93. Loening, A.M., Fenn, T.D., Wu, A.M., and Gambhir, S.S. (2006). Consensus guided mutagenesis of *Renilla* luciferase yields enhanced stability and light output. Protein Eng. Des. Sel. *19*, 391–400.

94. Zurkiya, O., Chan, A.W.S., and Hu, X. (2008). MagA is sufficient for producing magnetic nanoparticles in mammalian cells, making it an MRI reporter. Magn. Reson. Med. *59*, 1225–1231.

95. Cho, I.K., Moran, S.P., Paudyal, R., Piotrowska-Nitsche, K., Cheng, P.-H., Zhang, X., Mao, H., and Chan, A.W. (2014). Longitudinal monitoring of stem cell grafts in vivo using magnetic resonance imaging with inducible MagA as a genetic reporter. Theranostics *4*, 972–989.

96. Nakamura, C., Burgess, J.G., Sode, K., and Matsunaga, T. (1995). An iron-regulated gene, *magA*, encoding an iron transport protein of *Magnetospirillum* sp. strain AMB-1. J. Biol. Chem. *270*, 28392–28396.

97. Wu, M.-R., Huang, Y.-Y., and Hsiao, J.-K. (2019). Use of indocyanine green (ICG), a medical near infrared dye, for enhanced fluorescent imaging—comparison of organic anion transporting polypeptide 1B3 (OATP1B3) and sodium-taurocholate cotransporting polypeptide (NTCP) reporter genes. Molecules *24*, 2295.

98. Gilad, A.A., McMahon, M.T., Walczak, P., Winnard, P.T., Jr., Raman, V., van Laarhoven, H.W., Skoglund, C.M., Bulte, J.W., and van Zijl, P.C. (2007). Artificial reporter gene providing MRI contrast based on proton exchange. Nat. Biotechnol. *25*, 217–219.

99. Farrar, C.T., Buhrman, J.S., Liu, G., Kleijn, A., Lamfers, M.L., McMahon, M.T., Gilad, A.A., and Fulci, G. (2015). Establishing the lysine-rich protein CEST reporter gene as a CEST MR imaging detector for oncolytic virotherapy. Radiology *275*, 746–754.

100. Kremers, G.-J., Hazelwood, K.L., Murphy, C.S., Davidson, M.W., and Piston, D.W. (2009). Photoconversion in orange and red fluorescent proteins. Nat. Methods *6*, 355–358.

101. Lin, M.Z., McKeown, M.R., Ng, H.-L., Aguilera, T.A., Shaner, N.C., Campbell, R.E., Adams, S.R., Gross, L.A., Ma, W., Alber, T., and Tsien, R.Y. (2009). Autofluorescent proteins with excitation in the optical window for intravital imaging in mammals. Chem. Biol. *16*, 1169–1179.

102. Merzlyak, E.M., Goedhart, J., Shcherbo, D., Bulina, M.E., Shcheglov, A.S., Fradkov, A.F., Gaintzeva, A., Lukyanov, K.A., Lukyanov, S., Gadella, T.W., and Chudakov, D.M. (2007). Bright monomeric red fluorescent protein with an extended fluorescence lifetime. Nat. Methods *4*, 555–557.

103. Liu, M., Schmitner, N., Sandrian, M.G., Zabihian, B., Hermann, B., Salvenmoser, W., Meyer, D., and Drexler, W. (2013). In vivo three dimensional dual wavelength photoacoustic tomography imaging of the far red fluorescent protein E2-Crimson expressed in adult zebrafish. Biomed. Opt. Express *4*, 1846–1855.

104. Zhou, J., Sharkey, J., Shukla, R., Plagge, A., and Murray, P. (2017). Assessing the effectiveness of a far-red fluorescent reporter for tracking stem cells in vivo. Int. J. Mol. Sci. *19*, 19.

105. Shcherbakova, D.M., and Verkhusha, V.V. (2013). Near-infrared fluorescent proteins for multicolor in vivo imaging. Nat. Methods *10*, 751–754.

106. Shu, X., Royant, A., Lin, M.Z., Aguilera, T.A., Lev-Ram, V., Steinbach, P.A., and Tsien, R.Y. (2009). Mammalian expression of infrared fluorescent proteins engineered from a bacterial phytochrome. Science *324*, 804–807.

107. Filonov, G.S., Piatkevich, K.D., Ting, L.-M., Zhang, J., Kim, K., and Verkhusha, V.V. (2011). Bright and stable near-infrared fluorescent protein for in vivo imaging. Nat. Biotechnol. *29*, 757–761.

108. Deliolanis, N.C., Ale, A., Morscher, S., Burton, N.C., Schaefer, K., Radrich, K., Razansky, D., and Ntziachristos, V. (2014). Deep-tissue reporter-gene imaging with fluorescence and optoacoustic tomography: a performance overview. Mol. Imaging Biol. *16*, 652–660.

109. Wang, H., Willershäuser, M., Karlas, A., Gorpas, D., Reber, J., Ntziachristos, V., Maurer, S., Fromme, T., Li, Y., and Klingenspor, M. (2019). A dual *Ucp1* reporter mouse model for imaging and quantitation of brown and brite fat recruitment. Mol. Metab. *20*, 14–27.

110. Isomura, M., Yamada, K., Noguchi, K., and Nishizono, A. (2017). Near-infrared fluorescent protein iRFP720 is optimal for in vivo fluorescence imaging of rabies virus infection. J. Gen. Virol. *98*, 2689–2698.

111. Fukuda, A., Honda, S., Fujioka, N., Sekiguchi, Y., Mizuno, S., Miwa, Y., Sugiyama, F., Hayashi, Y., Nishimura, K., and Hisatake, K. (2019). Non-invasive in vivo imaging of UCP1 expression in live mice via near-infrared fluorescent protein iRFP720. PLoS ONE *14*, e0225213.

112. Farhadi, A., Ho, G.H., Sawyer, D.P., Bourdeau, R.W., and Shapiro, M.G. (2019). Ultrasound imaging of gene expression in mammalian cells. Science *365*, 1469–1475.

113. Bourdeau, R.W., Lee-Gosselin, A., Lakshmanan, A., Farhadi, A., Kumar, S.R., Nety, S.P., and Shapiro, M.G. (2018). Acoustic reporter genes for noninvasive imaging of microorganisms in mammalian hosts. Nature *553*, 86–90.

114. Goswami, R., Subramanian, G., Silayeva, L., Newkirk, I., Doctor, D., Chawla, K., Chattopadhyay, S., Chandra, D., Chilukuri, N., and Betapudi, V. (2019). Gene therapy leaves a vicious cycle. Front. Oncol. *9*, 297.

115. Ghani, K., Boivin-Welch, M., Roy, S., Dakiw-Piaceski, A., Barbier, M., Pope, E., Germain, L., and Caruso, M. (2019). Generation of high-titer self-inactivated γ-retroviral vector producer cells. Mol. Ther. Methods Clin. Dev. *14*, 90–99.

116. Ronald, J.A., Cusso, L., Chuang, H.Y., Yan, X., Dragulescu-Andrasi, A., and Gambhir, S.S. (2013). Development and validation of non-integrative, self-limited, and replicating minicircles for safe reporter gene imaging of cell-based therapies. PLoS ONE *8*, e73138.

117. Lufino, M.M., Edser, P.A., and Wade-Martins, R. (2008). Advances in high-capacity extrachromosomal vector technology: episomal maintenance, vector delivery, and transgene expression. Mol. Ther. *16*, 1525–1538.

118. Maggio, I., and Gonçalves, M.A. (2015). Genome editing at the crossroads of delivery, specificity, and fidelity. Trends Biotechnol. *33*, 280–291.

119. Bressan, R.B., Dewari, P.S., Kalantzaki, M., Gangoso, E., Matjusaitis, M., Garcia-Diaz, C., Blin, C., Grant, V., Bulstrode, H., Gogolok, S., et al. (2017). Efficient CRISPR/Cas9-assisted gene targeting enables rapid and precise genetic manipulation of mammalian neural stem cells. Development *144*, 635–648.

120. Lavaud, J., Henry, M., Coll, J.L., and Josserand, V. (2017). Exploration of melanoma metastases in mice brains using endogenous contrast photoacoustic imaging. Int. J. Pharm. *532*, 704–709.

121. Andreyev, A., and Celler, A. (2011). Dual-isotope PET using positron-gamma emitters. Phys. Med. Biol. *56*, 4539–4556.

122. Cal-González, J., Lage, E., Herranz, E., Vicente, E., Udias, J.M., Moore, S.C., Park, M.A., Dave, S.R., Parot, V., and Herraiz, J.L. (2015). Simulation of triple coincidences in PET. Phys. Med. Biol. *60*, 117–136.

123. Lage, E., Parot, V., Moore, S.C., Sitek, A., Udías, J.M., Dave, S.R., Park, M.A., Vaquero, J.J., and Herraiz, J.L. (2015). Recovery and normalization of triple coincidences in PET. Med. Phys. *42*, 1398–1410.

124. Zabow, G., Dodd, S., Moreland, J., and Koretsky, A. (2008). Micro-engineered local field control for high-sensitivity multispectral MRI. Nature *453*, 1058–1063.

125. O'Doherty, J., Jauregui-Osoro, M., Brothwood, T., Szyszko, T., Marsden, P.K., O'Doherty, M.J., Cook, G.J.R., Blower, P.J., and Lewington, V. (2017). $^{18}$F-tetrafluoroborate, a PET probe for imaging sodium/iodide symporter expression: whole-body biodistribution, safety, and radiation dosimetry in thyroid cancer patients. J. Nucl. Med. *58*, 1666–1671.

126. Fruhwirth, G.O., Diocou, S., Blower, P.J., Ng, T., and Mullen, G.E. (2014). A whole-body dual-modality radionuclide optical strategy for preclinical imaging of metastasis and heterogeneous treatment response in different microenvironments. J. Nucl. Med. *55*, 686–694.

127. Diocou, S., Volpe, A., Jauregui-Osoro, M., Boudjemeline, M., Chuamsaamarkkee, K., Man, F., Blower, P.J., Ng, T., Mullen, G.E.D., and Fruhwirth, G.O. (2017). [$^{18}$F]tetrafluoroborate-PET/CT enables sensitive tumor and metastasis in vivo imaging in a sodium iodide symporter-expressing tumor model. Sci. Rep. *7*, 946.

128. Moroz, M.A., Zhang, H., Lee, J., Moroz, E., Zurita, J., Shenker, L., Serganova, I., Blasberg, R., and Ponomarev, V. (2015). Comparative analysis of T cell imaging with human nuclear reporter genes. J. Nucl. Med. *56*, 1055–1060.

129. Ivashchenko, O., van der Have, F., Villena, J.L., Groen, H.C., Ramakers, R.M., Weinans, H.H., and Beekman, F.J. (2014). Quarter-millimeter-resolution molecular mouse imaging with U-SPECT$^{+}$. Mol. Imaging *13*.

130. Basu, S., Hess, S., Nielsen Braad, P.E., Olsen, B.B., Inglev, S., and Høilund-Carlsen, P.F. (2014). The basic principles of FDG-PET/CT imaging. PET Clin. *9*, 355–370, v.

131. Catana, C. (2017). Principles of simultaneous PET/MR imaging. Magn. Reson. Imaging Clin. N. Am. *25*, 231–243.

132. Khmelinskii, A., Meurer, M., Ho, C.T., Besenbeck, B., Füller, J., Lemberg, M.K., Bukau, B., Mogk, A., and Knop, M. (2016). Incomplete proteasomal degradation of green fluorescent proteins in the context of tandem fluorescent protein timers. Mol. Biol. Cell *27*, 360–370.

133. Subach, F.V., Subach, O.M., Gundorov, I.S., Morozova, K.S., Piatkevich, K.D., Cuervo, A.M., and Verkhusha, V.V. (2009). Monomeric fluorescent timers that change color from blue to red report on cellular trafficking. Nat. Chem. Biol. *5*, 118–126.

134. Terskikh, A., Fradkov, A., Ermakova, G., Zaraisky, A., Tan, P., Kajava, A.V., Zhao, X., Lukyanov, S., Matz, M., Kim, S., et al. (2000). "Fluorescent timer": protein that changes color with time. Science *290*, 1585–1588.

135. Misra, T., Baccino-Calace, M., Meyenhofer, F., Rodriguez-Crespo, D., Akarsu, H., Armenta-Calderón, R., Gorr, T.A., Frei, C., Cantera, R., Egger, B., and Luschnig, S. (2017). A genetically encoded biosensor for visualising hypoxia responses *in vivo*. Biol. Open *6*, 296–304.

136. Goldman, S.J., Chen, E., Taylor, R., Zhang, S., Petrosky, W., Reiss, M., and Jin, S. (2011). Use of the ODD-luciferase transgene for the non-invasive imaging of spontaneous tumors in mice. PLoS ONE *6*, e18269.

137. Cecic, I., Chan, D.A., Sutphin, P.D., Ray, P., Gambhir, S.S., Giaccia, A.J., and Graves, E.E. (2007). Oxygen sensitivity of reporter genes: implications for preclinical imaging of tumor hypoxia. Mol. Imaging *6*, 219–228.

138. Dohán, O., De la Vieja, A., Paroder, V., Riedel, C., Artani, M., Reed, M., Ginter, C.S., and Carrasco, N. (2003). The sodium/iodide Symporter (NIS): characterization, regulation, and medical significance. Endocr. Rev. *24*, 48–77.

139. Edmonds, S., Volpe, A., Shmeeda, H., Parente-Pereira, A.C., Radia, R., Baguña-Torres, J., Szanda, I., Severin, G.W., Livieratos, L., Blower, P.J., et al. (2016). Exploiting the metal-chelating properties of the drug cargo for in vivo positron emission tomography imaging of liposomal nanomedicines. ACS Nano *10*, 10294–10307.

140. Gambhir, S.S., Bauer, E., Black, M.E., Liang, Q., Kokoris, M.S., Barrio, J.R., Iyer, M., Namavari, M., Phelps, M.E., and Herschman, H.R. (2000). A mutant herpes simplex virus type 1 thymidine kinase reporter gene shows improved sensitivity for imaging reporter gene expression with positron emission tomography. Proc. Natl. Acad. Sci. USA *97*, 2785–2790.

141. Likar, Y., Dobrenkov, K., Olszewska, M., Shenker, L., Cai, S., Hricak, H., and Ponomarev, V. (2009). PET imaging of HSV1-tk mutants with acquired specificity toward pyrimidine- and acycloguanosine-based radiotracers. Eur. J. Nucl. Med. Mol. Imaging *36*, 1273–1282.

142. Yaghoubi, S.S., and Gambhir, S.S. (2006). PET imaging of herpes simplex virus type 1 thymidine kinase (HSV1-tk) or mutant HSV1-sr39tk reporter gene expression in mice and humans using [$^{18}$F]FHBG. Nat. Protoc. *1*, 3069–3075.

143. Tjuvajev, J.G., Doubrovin, M., Akhurst, T., Cai, S., Balatoni, J., Alauddin, M.M., Finn, R., Bornmann, W., Thaler, H., Conti, P.S., and Blasberg, R.G. (2002). Comparison of radiolabeled nucleoside probes (FIAU, FHBG, and FHPG) for PET imaging of HSV1-*tk* gene expression. J. Nucl. Med. *43*, 1072–1083.

144. Yusufi, N., Mall, S., Bianchi, H.O., Steiger, K., Reder, S., Klar, R., Audehm, S., Mustafa, M., Nekolla, S., Peschel, C., et al. (2017). In-depth characterization of a TCR-specific tracer for sensitive detection of tumor-directed transgenic T cells by immuno-PET. Theranostics *7*, 2402–2416.

145. Griessinger, C.M., Maurer, A., Kesenheimer, C., Kehlbach, R., Reischl, G., Ehrlichmann, W., Bukala, D., Harant, M., Cay, F., Brück, J., et al. (2015). $^{64}$Cu antibody-targeting of the T-cell receptor and subsequent internalization enables in vivo tracking of lymphocytes by PET. Proc. Natl. Acad. Sci. USA *112*, 1161–1166.

146. Larimer, B.M., Wehrenberg-Klee, E., Caraballo, A., and Mahmood, U. (2016). Quantitative CD3 PET imaging predicts tumor growth response to anti-CTLA-4 therapy. J. Nucl. Med. *57*, 1607–1611.

147. Seo, J.W., Tavaré, R., Mahakian, L.M., Silvestrini, M.T., Tam, S., Ingham, E.S., Salazar, F.B., Borowsky, A.D., Wu, A.M., and Ferrara, K.W. (2018). CD8$^{+}$ T-cell density imaging with $^{64}$Cu-Labeled cys-diabody informs immunotherapy protocols. Clin. Cancer Res. *24*, 4976–4987.

148. Freise, A.C., Zettlitz, K.A., Salazar, F.B., Lu, X., Tavaré, R., and Wu, A.M. (2017). ImmunoPET imaging of murine CD4$^{+}$ T cells using anti-CD4 cys-diabody: effects of protein dose on t cell function and imaging. Mol. Imaging Biol. *19*, 599–609.

149. Tavaré, R., Escuin-Ordinas, H., Mok, S., McCracken, M.N., Zettlitz, K.A., Salazar, F.B., Witte, O.N., Ribas, A., and Wu, A.M. (2016). An effective immuno-PET imaging method to monitor CD8-dependent responses to immunotherapy. Cancer Res. *76*, 73–82.

150. Ponomarev, V., Doubrovin, M., Lyddane, C., Beresten, T., Balatoni, J., Bornman, W., Finn, R., Akhurst, T., Larson, S., Blasberg, R., et al. (2001). Imaging TCR-dependent NFAT-mediated T-cell activation with positron emission tomography in vivo. Neoplasia *3*, 480–488.

151. Serganova, I., Cohen, I.J., Vemuri, K., Shindo, M., Maeda, M., Mane, M., Moroz, E., Khanin, R., Satagopan, J., Koutcher, J.A., and Blasberg, R. (2018). LDH-A regulates the tumor microenvironment via HIF-signaling and modulates the immune response. PLoS ONE *13*, e0203965.

152. Serganova, I., Doubrovin, M., Vider, J., Ponomarev, V., Soghomonyan, S., Beresten, T., Ageyeva, L., Serganov, A., Cai, S., Balatoni, J., et al. (2004). Molecular imaging of temporal dynamics and spatial heterogeneity of hypoxia-inducible factor-1 signal transduction activity in tumors in living mice. Cancer Res. *64*, 6101–6108.

153. Kleinovink, J.W., Mezzanotte, L., Zambito, G., Fransen, M.F., Cruz, L.J., Verbeek, J.S., Chan, A., Ossendorp, F., and Löwik, C. (2019). A dual-color bioluminescence reporter mouse for simultaneous *in vivo* imaging of T cell localization and function. Front. Immunol. *9*, 3097.

154. Brown, C.E., Warden, C.D., Starr, R., Deng, X., Badie, B., Yuan, Y.C., Forman, S.J., and Barish, M.E. (2013). Glioma IL13Rα2 is associated with mesenchymal signature gene expression and poor patient prognosis. PLoS ONE *8*, e77769.

155. Keu, K.V., Witney, T.H., Yaghoubi, S., Rosenberg, J., Kurien, A., Magnusson, R., Williams, J., Habte, F., Wagner, J.R., Forman, S., et al. (2017). Reporter gene imaging of targeted T cell immunotherapy in recurrent glioma. Sci. Transl. Med. *9*, eaag2196.

156. Berger, C., Flowers, M.E., Warren, E.H., and Riddell, S.R. (2006). Analysis of transgene-specific immune responses that limit the in vivo persistence of adoptively transferred HSV-TK-modified donor T cells after allogeneic hematopoietic cell transplantation. Blood *107*, 2294–2302.

157. Zhang, H., Moroz, M.A., Serganova, I., Ku, T., Huang, R., Vider, J., Maecke, H.R., Larson, S.M., Blasberg, R., and Smith-Jones, P.M. (2011). Imaging expression of the human somatostatin receptor subtype-2 reporter gene with $^{68}$Ga-DOTATOC. J. Nucl. Med. *52*, 123–131.

158. Vedvyas, Y., Shevlin, E., Zaman, M., Min, I.M., Amor-Coarasa, A., Park, S., Park, S., Kwon, K.W., Smith, T., Luo, Y., et al. (2016). Longitudinal PET imaging demonstrates biphasic CAR T cell responses in survivors. JCI Insight *1*, e90064.

159. Yamada, Y., Post, S.R., Wang, K., Tager, H.S., Bell, G.I., and Seino, S. (1992). Cloning and functional characterization of a family of human and mouse somatostatin receptors expressed in brain, gastrointestinal tract, and kidney. Proc. Natl. Acad. Sci. USA *89*, 251–255.

160. Elliott, D.E., Li, J., Blum, A.M., Metwali, A., Patel, Y.C., and Weinstock, J.V. (1999). SSTR2A is the dominant somatostatin receptor subtype expressed by inflammatory cells, is widely expressed and directly regulates T cell IFN-gamma release. Eur. J. Immunol. *29*, 2454–2463.

161. Barsegian, V., Hueben, C., Mueller, S.P., Poeppel, T.D., Horn, P.A., Bockisch, A., and Lindemann, M. (2015). Impairment of lymphocyte function following yttrium-90 DOTATOC therapy. Cancer Immunol. Immunother. *64*, 755–764.

162. Cescato, R., Schulz, S., Waser, B., Eltschinger, V., Rivier, J.E., Wester, H.J., Culler, M., Ginj, M., Liu, Q., Schonbrunn, A., and Reubi, J.C. (2006). Internalization of $sst_2$, $sst_3$, and $sst_5$ receptors: effects of somatostatin agonists and antagonists. J. Nucl. Med. *47*, 502–511.

163. Oomen, S.P., Hofland, L.J., Lamberts, S.W., Löwenberg, B., and Touw, I.P. (2001). Internalization-defective mutants of somatostatin receptor subtype 2 exert normal signaling functions in hematopoietic cells. FEBS Lett. *503*, 163–167.

164. Groot-Wassink, T., Aboagye, E.O., Wang, Y., Lemoine, N.R., Keith, W.N., and Vassaux, G. (2004). Noninvasive imaging of the transcriptional activities of human telomerase promoter fragments in mice. Cancer Res. *64*, 4906–4911.

165. Sieger, S., Jiang, S., Schönsiegel, F., Eskerski, H., Kübler, W., Altmann, A., and Haberkorn, U. (2003). Tumour-specific activation of the sodium/iodide symporter gene under control of the glucose transporter gene 1 promoter (GTI-1.3). Eur. J. Nucl. Med. Mol. Imaging *30*, 748–756.

166. Merron, A., Peerlinck, I., Martin-Duque, P., Burnet, J., Quintanilla, M., Mather, S., Hingorani, M., Harrington, K., Iggo, R., and Vassaux, G. (2007). SPECT/CT imaging of oncolytic adenovirus propagation in tumours in vivo using the Na/I symporter as a reporter gene. Gene Ther. *14*, 1731–1738.

167. Dingli, D., Kemp, B.J., O'Connor, M.K., Morris, J.C., Russell, S.J., and Lowe, V.J. (2006). Combined I-124 positron emission tomography/computed tomography imaging of NIS gene expression in animal models of stably transfected and intravenously transfected tumor. Mol. Imaging Biol. *8*, 16–23.

168. Carlson, S.K., Classic, K.L., Hadac, E.M., Dingli, D., Bender, C.E., Kemp, B.J., and Russell, S.J. (2009). Quantitative molecular imaging of viral therapy for pancreatic cancer using an engineered measles virus expressing the sodium-iodide symporter reporter gene. AJR Am. J. Roentgenol. *192*, 279–287.

169. Higuchi, T., Anton, M., Saraste, A., Dumler, K., Pelisek, J., Nekolla, S.G., Bengel, F.M., and Schwaiger, M. (2009). Reporter gene PET for monitoring survival of transplanted endothelial progenitor cells in the rat heart after pretreatment with VEGF and atorvastatin. J. Nucl. Med. *50*, 1881–1886.

170. Terrovitis, J., Kwok, K.F., Lautamäki, R., Engles, J.M., Barth, A.S., Kizana, E., Miake, J., Leppo, M.K., Fox, J., Seidel, J., et al. (2008). Ectopic expression of the sodium-iodide symporter enables imaging of transplanted cardiac stem cells in vivo by single-photon emission computed tomography or positron emission tomography. J. Am. Coll. Cardiol. *52*, 1652–1660.

171. Che, J., Doubrovin, M., Serganova, I., Ageyeva, L., Zanzonico, P., and Blasberg, R. (2005). hNIS-IRES-eGFP dual reporter gene imaging. Mol. Imaging *4*, 128–136.

172. Ashmore-Harris, C., Blackford, S.J., Grimsdell, B., Kurtys, E., Glatz, M.C., Rashid, T.S., and Fruhwirth, G.O. (2019). Reporter gene-engineering of human induced pluripotent stem cells during differentiation renders in vivo traceable hepatocyte-like cells accessible. Stem Cell Res. (Amst.) *41*, 101599.

173. Kurtys, E., Lim, L., Man, F., Volpe, A., and Fruhwirth, G. (2018). In vivo tracking of CAR-T by [$^{18}$f]$BF_4^-$ PET/CT in human breast cancer xenografts reveals differences in CAR-T tumour retention. Cytotherapy *20* (*Suppl*), S20.

174. Emami-Shahri, N., Foster, J., Kashani, R., Gazinska, P., Cook, C., Sosabowski, J., Maher, J., and Papa, S. (2018). Clinically compliant spatial and temporal imaging of chimeric antigen receptor T-cells. Nat. Commun. *9*, 1081.

175. O'Keefe, D.S., Bacich, D.J., Huang, S.S., and Heston, W.D.W. (2018). A perspective on the evolving story of PSMA biology, PSMA-based imaging, and endoradiotherapeutic strategies. J. Nucl. Med. *59*, 1007–1013.

176. Liu, H., Rajasekaran, A.K., Moy, P., Xia, Y., Kim, S., Navarro, V., Rahmati, R., and Bander, N.H. (1998). Constitutive and antibody-induced internalization of prostate-specific membrane antigen. Cancer Res. *58*, 4055–4060.

177. Rajasekaran, S.A., Anilkumar, G., Oshima, E., Bowie, J.U., Liu, H., Heston, W., Bander, N.H., and Rajasekaran, A.K. (2003). A novel cytoplasmic tail MXXXL motif mediates the internalization of prostate-specific membrane antigen. Mol. Biol. Cell *14*, 4835–4845.

178. Corneillie, T.M., Whetstone, P.A., Lee, K.C., Wong, J.P., and Meares, C.F. (2004). Converting weak binders into infinite binders. Bioconjug. Chem. *15*, 1389–1391.

179. Goodwin, D.A., Meares, C.F., Watanabe, N., McTigue, M., Chaovapong, W., Ransone, C.M., Renn, O., Greiner, D.P., Kukis, D.L., and Kronenberger, S.I. (1994). Pharmacokinetics of pretargeted monoclonal antibody 2D12.5 and $^{88}$Y-Janus-2-(*p*-nitrobenzyl)-1,4,7,10-tetraazacyclododecanetetraacetic acid (DOTA) in BALB/c mice with KHJJ mouse adenocarcinoma: a model for $^{90}$Y radioimmunotherapy. Cancer Res. *54*, 5937–5946.

180. Lubberink, M., and Herzog, H. (2011). Quantitative imaging of $^{124}$I and $^{86}$Y with PET. Eur. J. Nucl. Med. Mol. Imaging *38* (*Suppl 1*), S10–S18.

181. Di Stasi, A., Tey, S.K., Dotti, G., Fujita, Y., Kennedy-Nasser, A., Martinez, C., Straathof, K., Liu, E., Durett, A.G., Grilley, B., et al. (2011). Inducible apoptosis as a safety switch for adoptive cell therapy. N. Engl. J. Med. *365*, 1673–1683.

182. Itakura, G., Kawabata, S., Ando, M., Nishiyama, Y., Sugai, K., Ozaki, M., Iida, T., Ookubo, T., Kojima, K., Kashiwagi, R., et al. (2017). Fail-safe system against potential tumorigenicity after transplantation of iPSC derivatives. Stem Cell Reports *8*, 673–684.

183. Philip, B., Kokalaki, E., Mekkaoui, L., Thomas, S., Straathof, K., Flutter, B., Marin, V., Marafioti, T., Chakraverty, R., Linch, D., et al. (2014). A highly compact epitope-based marker/suicide gene for easier and safer T-cell therapy. Blood *124*, 1277–1287.

184. Wang, X., Chang, W.C., Wong, C.W., Colcher, D., Sherman, M., Ostberg, J.R., Forman, S.J., Riddell, S.R., and Jensen, M.C. (2011). A transgene-encoded cell surface polypeptide for selection, in vivo tracking, and ablation of engineered cells. Blood *118*, 1255–1263.

185. Stavrou, M., Philip, B., Traynor-White, C., Davis, C.G., Onuoha, S., Cordoba, S., Thomas, S., and Pule, M. (2018). A rapamycin-activated caspase 9-based suicide gene. Mol. Ther. *26*, 1266–1276.

186. Boardman, D.A., Philippeos, C., Fruhwirth, G.O., Ibrahim, M.A., Hannen, R.F., Cooper, D., Marelli-Berg, F.M., Watt, F.M., Lechler, R.I., Maher, J., et al. (2017). Expression of a chimeric antigen receptor specific for donor HLA class I enhances the potency of human regulatory T cells in preventing human skin transplant rejection. Am. J. Transplant. *17*, 931–943.

187. Safinia, N., Vaikunthanathan, T., Fraser, H., Thirkell, S., Lowe, K., Blackmore, L., Whitehouse, G., Martinez-Llordella, M., Jassem, W., Sanchez-Fueyo, A., et al. (2016). Successful expansion of functional and stable regulatory T cells for immunotherapy in liver transplantation. Oncotarget *7*, 7563–7577.

188. Scottà, C., Esposito, M., Fazekasova, H., Fanelli, G., Edozie, F.C., Ali, N., Xiao, F., Peakman, M., Afzali, B., Sagoo, P., et al. (2013). Differential effects of rapamycin and retinoic acid on expansion, stability and suppressive qualities of human $CD4^+CD25^+FOXP3^+$ T regulatory cell subpopulations. Haematologica *98*, 1291–1299.

189. Caplan, A.I. (2019). Medicinal signalling cells: they work, so use them. Nature *566*, 39.

190. Zhu, J., Zhou, L., and XingWu, F. (2006). Tracking neural stem cells in patients with brain trauma. N. Engl. J. Med. *355*, 2376–2378.

191. Karussis, D., Karageorgiou, C., Vaknin-Dembinsky, A., Gowda-Kurkalli, B., Gomori, J.M., Kassis, I., Bulte, J.W., Petrou, P., Ben-Hur, T., Abramsky, O., and Slavin, S. (2010). Safety and immunological effects of mesenchymal stem cell transplantation in patients with multiple sclerosis and amyotrophic lateral sclerosis. Arch. Neurol. *67*, 1187–1194.

192. Gholamrezanezhad, A., Mirpour, S., Bagheri, M., Mohamadnejad, M., Alimoghaddam, K., Abdolahzadeh, L., Saghari, M., and Malekzadeh, R. (2011). In vivo tracking of $^{111}$In-oxine labeled mesenchymal stem cells following infusion in patients with advanced cirrhosis. Nucl. Med. Biol. *38*, 961–967.

193. Kang, W.J., Kang, H.J., Kim, H.S., Chung, J.K., Lee, M.C., and Lee, D.S. (2006). Tissue distribution of $^{18}$F-FDG-labeled peripheral hematopoietic stem cells after intracoronary administration in patients with myocardial infarction. J. Nucl. Med. *47*, 1295–1301.

194. Hofmann, M., Wollert, K.C., Meyer, G.P., Menke, A., Arseniev, L., Hertenstein, B., Ganser, A., Knapp, W.H., and Drexler, H. (2005). Monitoring of bone marrow cell homing into the infarcted human myocardium. Circulation *111*, 2198–2202.

195. Vrtovec, B., Poglajen, G., Lezaic, L., Sever, M., Socan, A., Domanovic, D., Cernelc, P., Torre-Amione, G., Haddad, F., and Wu, J.C. (2013). Comparison of transendocardial and intracoronary $CD34^+$ cell transplantation in patients with nonischemic dilated cardiomyopathy. Circulation *128* (11, Suppl 1), S42–S49.

196. Wu, J.C., Chen, I.Y., Sundaresan, G., Min, J.J., De, A., Qiao, J.H., Fishbein, M.C., and Gambhir, S.S. (2003). Molecular imaging of cardiac cell transplantation in living animals using optical bioluminescence and positron emission tomography. Circulation *108*, 1302–1305.

197. Pei, Z., Lan, X., Cheng, Z., Qin, C., Wang, P., He, Y., Yen, T.C., Tian, Y., Mghanga, F.P., and Zhang, Y. (2012). A multimodality reporter gene for monitoring transplanted stem cells. Nucl. Med. Biol. *39*, 813–820.

198. Lee, A.S., Tang, C., Cao, F., Xie, X., van der Bogt, K., Hwang, A., Connolly, A.J., Robbins, R.C., and Wu, J.C. (2009). Effects of cell number on teratoma formation by human embryonic stem cells. Cell Cycle *8*, 2608–2612.

199. Pomper, M.G., Hammond, H., Yu, X., Ye, Z., Foss, C.A., Lin, D.D., Fox, J.J., and Cheng, L. (2009). Serial imaging of human embryonic stem-cell engraftment and teratoma formation in live mouse models. Cell Res. *19*, 370–379.

200. McCracken, M.N., Gschweng, E.H., Nair-Gill, E., McLaughlin, J., Cooper, A.R., Riedinger, M., Cheng, D., Nosala, C., Kohn, D.B., and Witte, O.N. (2013). Long-term in vivo monitoring of mouse and human hematopoietic stem cell engraftment with a human positron emission tomography reporter gene. Proc. Natl. Acad. Sci. USA *110*, 1857–1862.

201. Kim, Y.H., Lee, D.S., Kang, J.H., Lee, Y.J., Chung, J.-K., Roh, J.-K., Kim, S.U., and Lee, M.C. (2005). Reversing the silencing of reporter sodium/iodide symporter transgene for stem cell tracking. J. Nucl. Med. *46*, 305–311.

202. Schug, C., Urnauer, S., Jaeckel, C., Schmohl, K.A., Tutter, M., Steiger, K., Schwenk, N., Schwaiger, M., Wagner, E., Nelson, P.J., and Spitzweg, C. (2019). TGFB1-driven mesenchymal stem cell-mediated NIS gene transfer. Endocr. Relat. Cancer *26*, 89–101.

203. Dwyer, R.M., Ryan, J., Havelin, R.J., Morris, J.C., Miller, B.W., Liu, Z., Flavin, R., O'Flatharta, C., Foley, M.J., Barrett, H.H., et al. (2011). Mesenchymal stem cell-mediated delivery of the sodium iodide symporter supports radionuclide imaging and treatment of breast cancer. Stem Cells *29*, 1149–1157.

204. Love, Z., Wang, F., Dennis, J., Awadallah, A., Salem, N., Lin, Y., Weisenberger, A., Majewski, S., Gerson, S., and Lee, Z. (2007). Imaging of mesenchymal stem cell transplant by bioluminescence and PET. J. Nucl. Med. *48*, 2011–2020.

205. Schönitzer, V., Haasters, F., Käsbauer, S., Ulrich, V., Mille, E., Gildehaus, F.J., Carlsen, J., Pape, M., Beck, R., Delker, A., et al. (2014). In vivo mesenchymal stem cell tracking with PET using the dopamine type 2 receptor and $^{18}$F-fallypride. J. Nucl. Med. *55*, 1342–1347.

206. Willmann, J.K., Paulmurugan, R., Rodriguez-Porcel, M., Stein, W., Brinton, T.J., Connolly, A.J., Nielsen, C.H., Lutz, A.M., Lyons, J., Ikeno, F., et al. (2009). Imaging gene expression in human mesenchymal stem cells: from small to large animals. Radiology *252*, 117–127.

207. Swijnenburg, R.-J., Schrepfer, S., Govaert, J.A., Cao, F., Ransohoff, K., Sheikh, A.Y., Haddad, M., Connolly, A.J., Davis, M.M., Robbins, R.C., and Wu, J.C. (2008). Immunosuppressive therapy mitigates immunological rejection of human embryonic stem cell xenografts. Proc. Natl. Acad. Sci. USA *105*, 12991–12996.

208. Daadi, M.M., Hu, S., Klausner, J., Li, Z., Sofilos, M., Sun, G., Wu, J.C., and Steinberg, G.K. (2013). Imaging neural stem cell graft-induced structural repair in stroke. Cell Transplant. *22*, 881–892.

209. Priddle, H., Grabowska, A., Morris, T., Clarke, P.A., McKenzie, A.J., Sottile, V., Denning, C., Young, L., and Watson, S. (2009). Bioluminescence imaging of human embryonic stem cells transplanted in vivo in murine and chick models. Cloning Stem Cells *11*, 259–267.

210. Wolfs, E., Holvoet, B., Ordovas, L., Breuls, N., Helsen, N., Schönberger, M., Raitano, S., Struys, T., Vanbilloen, B., Casteels, C., et al. (2017). Molecular imaging of human embryonic stem cells stably expressing human PET reporter genes after zinc finger nuclease-mediated genome editing. J. Nucl. Med. *58*, 1659–1665.

211. Wang, Y., Zhang, W.Y., Hu, S., Lan, F., Lee, A.S., Huber, B., Lisowski, L., Liang, P., Huang, M., de Almeida, P.E., et al. (2012). Genome editing of human embryonic stem cells and induced pluripotent stem cells with zinc finger nucleases for cellular imaging. Circ. Res. *111*, 1494–1503.

212. Tian, X., Hexum, M.K., Penchev, V.R., Taylor, R.J., Shultz, L.D., and Kaufman, D.S. (2009). Bioluminescent imaging demonstrates that transplanted human embryonic stem cell-derived $CD34^+$ cells preferentially develop into endothelial cells. Stem Cells *27*, 2675–2685.

213. Laurila, J.P., Laatikainen, L., Castellone, M.D., Trivedi, P., Heikkila, J., Hinkkanen, A., Hematti, P., and Laukkanen, M.O. (2009). Human embryonic stem cell-derived mesenchymal stromal cell transplantation in a rat hind limb injury model. Cytotherapy *11*, 726–737.

214. Li, Z., Suzuki, Y., Huang, M., Cao, F., Xie, X., Connolly, A., et al. (2008). Comparison of Reporter Gene and Iron Particle Labeling for Tracking Fate of Human Embryonic Stem Cells and Differentiated Endothelial Cells in Living Subjects. Stem Cells *26*, 864–873, https://doi.org/10.1634/stemcells.2007-0843.

215. Bradbury, M.S., Panagiotakos, G., Chan, B.K., Tomishima, M., Zanzonico, P., Vider, J., Ponomarev, V., Studer, L., and Tabar, V. (2007). Optical bioluminescence imaging of human ES cell progeny in the rodent CNS. J. Neurochem. *102*, 2029–2039.

216. Barberi, T., Bradbury, M., Dincer, Z., Panagiotakos, G., Socci, N.D., and Studer, L. (2007). Derivation of engraftable skeletal myoblasts from human embryonic stem cells. Nat. Med. *13*, 642–648.

217. Lopez-Yrigoyen, M., Fidanza, A., Cassetta, L., Axton, R.A., Taylor, A.H., Meseguer-Ripolles, J., Tsakiridis, A., Wilson, V., Hay, D.C., Pollard, J.W., and Forrester, L.M. (2018). A human iPSC line capable of differentiating into functional macrophages expressing ZsGreen: a tool for the study and *in vivo* tracking of therapeutic cells. Philos. Trans. R. Soc. Lond. B Biol. Sci. *373*, 20170219.

218. Itakura, G., Kobayashi, Y., Nishimura, S., Iwai, H., Takano, M., Iwanami, A., Toyama, Y., Okano, H., and Nakamura, M. (2015). Controlling immune rejection is a fail-safe system against potential tumorigenicity after human iPSC-derived neural stem cell transplantation. PLoS ONE *10*, e0116413.

219. Rufaihah, A.J., Huang, N.F., Jamé, S., Lee, J.C., Nguyen, H.N., Byers, B., De, A., Okogbaa, J., Rollins, M., Reijo-Pera, R., et al. (2011). Endothelial cells derived from human iPSCS increase capillary density and improve perfusion in a mouse model of peripheral arterial disease. Arterioscler. Thromb. Vasc. Biol. *31*, e72–e79.

220. Templin, C., Zweigerdt, R., Schwanke, K., Olmer, R., Ghadri, J.-R., Emmert, M.Y., Müller, E., Küest, S.M., Cohrs, S., Schibli, R., et al. (2012). Transplantation and

tracking of human-induced pluripotent stem cells in a pig model of myocardial infarction: assessment of cell survival, engraftment, and distribution by hybrid single photon emission computed tomography/computed tomography of sodium iodide symporter transgene expression. Circulation *126*, 430–439.

221. Bedel, A., Beliveau, F., Lamrissi-Garcia, I., Rousseau, B., Moranvillier, I., Rucheton, B., Guyonnet-Dupérat, V., Cardinaud, B., de Verneuil, H., Moreau-Gaudry, F., and Dabernat, S. (2017). Preventing pluripotent cell teratoma in regenerative medicine applied to hematology disorders. Stem Cells Transl. Med. *6*, 382–393.

222. Mattapally, S., Zhu, W., Fast, V.G., Gao, L., Worley, C., Kannappan, R., Borovjagin, A.V., and Zhang, J. (2018). Spheroids of cardiomyocytes derived from human-induced pluripotent stem cells improve recovery from myocardial injury in mice. Am. J. Physiol. Heart Circ. Physiol. *315*, H327–H339.

223. Volarevic, V., Markovic, B.S., Gazdic, M., Volarevic, A., Jovicic, N., Arsenijevic, N., Armstrong, L., Djonov, V., Lako, M., and Stojkovic, M. (2018). Ethical and safety issues of stem cell-based therapy. Int. J. Med. Sci. *15*, 36–45.

224. Oceguera-Yanez, F., Kim, S.I., Matsumoto, T., Tan, G.W., Xiang, L., Hatani, T., Kondo, T., Ikeya, M., Yoshida, Y., Inoue, H., and Woltjen, K. (2016). Engineering the AAVS1 locus for consistent and scalable transgene expression in human iPSCs and their differentiated derivatives. Methods *101*, 43–55.

225. Thomson, J.A., Itskovitz-Eldor, J., Shapiro, S.S., Waknitz, M.A., Swiergiel, J.J., Marshall, V.S., and Jones, J.M. (1998). Embryonic stem cell lines derived from human blastocysts. Science *282*, 1145–1147.

226. Tosca, L., Feraud, O., Magniez, A., Bas, C., Griscelli, F., Bennaceur-Griscelli, A., and Tachdjian, G. (2015). Genomic instability of human embryonic stem cell lines using different passaging culture methods. Mol. Cytogenet. *8*, 30.

227. Huang, C.Y., Liu, C.L., Ting, C.Y., Chiu, Y.T., Cheng, Y.C., Nicholson, M.W., and Hsieh, P.C.H. (2019). Human iPSC banking: barriers and opportunities. J. Biomed. Sci. *26*, 87.

228. Charoenphun, P., Meszaros, L.K., Chuamsaamarkkee, K., Sharif-Paghaleh, E., Ballinger, J.R., Ferris, T.J., Went, M.J., Mullen, G.E., and Blower, P.J. (2015). [$^{89}$Zr]oxinate4 for long-term in vivo cell tracking by positron emission tomography. Eur. J. Nucl. Med. Mol. Imaging *42*, 278–287.

229. Sato, N., Wu, H., Asiedu, K.O., Szajek, L.P., Griffiths, G.L., and Choyke, P.L. (2015). $^{89}$Zr-oxine complex PET cell imaging in monitoring cell-based therapies. Radiology *275*, 490–500.

230. Man, F., Lim, L., Volpe, A., Gabizon, A., Shmeeda, H., Draper, B., Parente-Pereira, A.C., Maher, J., Blower, P.J., Fruhwirth, G.O., and T M de Rosales, R. (2019). In vivo PET tracking of $^{89}$Zr-labeled Vγ9Vδ2 T cells to mouse xenograft breast tumors activated with liposomal alendronate. mol. Ther. *27*, 219–229.

231. Cherry, S.R., Jones, T., Karp, J.S., Qi, J., Moses, W.W., and Badawi, R.D. (2018). Total-body PET: maximizing sensitivity to create new opportunities for clinical research and patient care. J. Nucl. Med. *59*, 3–12.

232. Eyquem, J., Mansilla-Soto, J., Giavridis, T., van der Stegen, S.J., Hamieh, M., Cunanan, K.M., Odak, A., Gönen, M., and Sadelain, M. (2017). Targeting a CAR to the TRAC locus with CRISPR/Cas9 enhances tumour rejection. Nature *543*, 113–117.

233. Kotterman, M.A., Chalberg, T.W., and Schaffer, D.V. (2015). Viral vectors for gene therapy: translational and clinical outlook. Annu. Rev. Biomed. Eng. *17*, 63–89.

234. Martinez, M., and Moon, E.K. (2019). CAR T cells for solid tumors: new strategies for finding, infiltrating, and surviving in the tumor microenvironment. Front. Immunol. *10*, 128.

235. Naumova, A.V., Modo, M., Moore, A., Murry, C.E., and Frank, J.A. (2014). Clinical imaging in regenerative medicine. Nat. Biotechnol. *32*, 804–818.

236. Afzali, B., Edozie, F.C., Fazekasova, H., Scottà, C., Mitchell, P.J., Canavan, J.B., Kordasti, S.Y., Chana, P.S., Ellis, R., Lord, G.M., et al. (2013). Comparison of regulatory T cells in hemodialysis patients and healthy controls: implications for cell therapy in transplantation. Clin. J. Am. Soc. Nephrol. *8*, 1396–1405.

237. Alhadj Ali, M., Liu, Y.F., Arif, S., Tatovic, D., Shariff, H., Gibson, V.B., Yusuf, N., Baptista, R., Eichmann, M., Petrov, N., et al. (2017). Metabolic and immune effects of immunotherapy with proinsulin peptide in human new-onset type 1 diabetes. Sci. Transl. Med. *9*, eaaf7779.

238. Smith, E.L., and Peakman, M. (2018). Peptide immunotherapy for type 1 diabetes-clinical advances. Front. Immunol. *9*, 392.

239. Chataway, J., Martin, K., Barrell, K., Sharrack, B., Stolt, P., and Wraith, D.C.; ATX-MS1467 Study Group (2018). Effects of ATX-MS-1467 immunotherapy over 16 weeks in relapsing multiple sclerosis. Neurology *90*, e955–e962.

240. Hotchkiss, R.S., and Moldawer, L.L. (2014). Parallels between cancer and infectious disease. N. Engl. J. Med. *371*, 380–383.